Tuning vortex fluctuations and the resistive transition in superconducting films with a thin overlayer

Alex Gurevich[*]

Department of Physics, Old Dominion University, Norfolk, Virginia 23529, USA

It is shown that the temperature of the resistive transition T_r of a superconducting film can be increased by a thin superconducting or normal overlayer. For instance, deposition of a highly conductive thin overlayer onto a dirty superconducting film can give rise to an "antiproximity effect," which manifests itself in an initial increase of $T_r(d_2)$ with the overlayer thickness d_2 followed by a decrease of $T_r(d_2)$ at larger d_2. Such a nonmonotonic thickness dependence of $T_r(d_2)$ results from the interplay of the increase of a net superfluid density mitigating phase fluctuations and the suppression of the critical temperature T_c due to the conventional proximity effect. This behavior of $T_r(d_2)$ is obtained by solving the Usadel equations to calculate the temperature of the Berezinskii-Kosterlitz-Thouless transition, and the temperature of the resistive transition due to thermally activated hopping of single vortices in dirty bilayers. The theory incorporates relevant material parameters such as thicknesses and conductivities of the layers, the interface contact resistance between them, and the subgap quasiparticle states, which affect both phase fluctuations and the proximity effect suppression of T_c. The transition temperature T_r can be optimized by tuning the overlayer parameters, which can significantly weaken vortex fluctuations and nearly restore the mean-field critical temperature. The calculated behavior of $T_r(d_2)$ may explain the nonmonotonic dependence of $T_r(d_2)$ observed on (Ag,Au,Mg,Zn)-coated Bi films, Ag-coated Ga and Pb films, or NbN and NbTiN films on AlN buffer layers. These results suggest that bilayers can be used as model systems for systematic investigations of optimization of fluctuations in superconductors.

I. INTRODUCTION

Recent discoveries of two-dimensional (2D) materials and interfaces with unique physical properties [1–6], particularly the observations of superconductivity in FeSe monolayers on strontium titanate [7–13], monolayers of Pb on Si substrates [14–16], or 2H TaS$_2$ [17] have renewed the interest in the pairing mechanisms and the effect of vortex fluctuations in extreme 2D superconductors. In addition to the complex physics of charge transfer, strain effects, and collective excitations at the interfaces, the observation of a superconducting transition and the opening of the quasiparticle gap in FeSe monolayers at temperatures over 100 K brings about the following issue. The observed temperature of the resistive transition T_r in a superconducting monolayer is always reduced by pair-breaking fluctuations of the order parameter and the Berezinskii-Kosterlitz-Thouless (BKT) proliferation of vortices [18,19], which should be particularly pronounced in dirty thin films such as amorphous Pb monolayers [14–16] or FeSe monolayers with low superfluid density and the Fermi energies $E_F \simeq 10$–100 meV [1–6]. In that case, a mean-field pairing temperature T_c would be expected to be well above the observed $T_r \simeq 50$ K. The question, then, is what is the actual T_c and to what extent can it be restored by reducing fluctuations by materials nanostructuring?

Pair-breaking fluctuations can be mitigated by enhancing the phase stiffness, which implies increasing the superfluid density or reducing the quasiparticle mass or electronic anisotropy [20,21]. It has been proposed to do so by combining strongly fluctuating superconducting layers with a nonsuperconducting material with high carrier density [22,23]. Using the Hubbard model for a superconducting (S) layer coupled to a normal (N) layer, it was shown that this mechanism can increase the phase stiffness in the bilayer and increase the transition temperature [22,23]. Yet testing this proposal experimentally would require a theory in which the observed T_r in a bilayer is expressed in terms of accessible material parameters such as thicknesses and conductivities of the S and N layers, and an interface contact resistance that can be readily tuned to optimize both the phase fluctuations and the proximity effect suppression of T_c. Such an approach is developed in this work in which the resistive transition is associated with the BKT transition temperature T_b or the temperature of the resistive transition caused by thermally activated hopping of vortices. These transition temperatures were calculated here using the theory of the proximity effect in dirty thin-film bilayers described by the Usadel equations [24–29]. The theory shows that $T_r(d_2)$ first increases with the thickness of a conductive overlayer d_2, reaches a maximum that can be rather close to T_c, and then decreases as d_2 further increases. Such behavior of $T_r(d_2)$ resulting from the interplay of an enhanced phase stiffness and a reduction of T_c due to the proximity effect occurs if the conductivity of the overlayer is much higher than the conductivity of the S film in the normal state. In this case, T_r reaches maximum at the overlayer thicknesses much smaller than the thickness of the S film.

The above mechanism may be relevant to the nonmonotonic dependencies of the resistive transition temperatures of ultrathin films on the thickness of conductive overlayers observed

*gurevich@odu.edu

024506-1

on (Ag, Au, Mg, Zn)-coated Bi films [30,31], Ag-coated Ga [32] and Pb films [33], or NbN and NbTiN films on AlN buffer layers [34]. It was also observed that T_r of La$_{2-x}$Sr$_x$CuO$_4$ thin films capped by an overdoped metallic La$_{1.65}$Sr$_{0.35}$CuO$_4$ layer is higher than T_c of the bare film, indicating the effect of enhanced phase stiffness [35]. Other experiments revealed the effect of disconnected metallic gates on T_r of the 2D arrays of Al Josephson junctions [36] and amorphous MoGe films [37]. Subsequent theories associated the effect of remote N overlayers on T_r with a tunable dissipative environment affecting fluctuations of the order parameter that drive a superconductor-insulator transition [38] and quantum tunneling of vortices [39] through either capacitive or inductive coupling with the metallic gates. It was also proposed to tune the BKT transition temperature with a decoupled thick S overlayer [40]. Other mechanisms of the nonmonotonic dependence of $T_r(d_2)$ may be related to a broader issue of interface superconductivity [41,42] or the reduction of the Coulomb repulsion in the S film by a thin N overlayer [43,44].

In this work, the effect of a thin overlayer on vortex fluctuations in a thin film is addressed, assuming that the overlayer is in contact with the film. Here the effect of the overlayer on T_r is associated with an increased energy of a perpendicular vortex. In this case, restoring the mean-field T_c could be achieved by depositing not only a highly conductive N overlayer but also an S overlayer with higher T_c coupled through a Josephson buffer junction, for instance a Bi-2223 or YBCO overlayer onto the FeSe monolayer. Such a high-T_c overlayer would be particularly effective to suppress the BKT fluctuations in a lower-T_c layer. Overlayers can also be used to reduce the effect of vortex fluctuations in granular films of arrays of Josephson junctions. A model developed here incorporates material features into a theory of the BKT transition in a proximity-coupled bilayer. This model primarily focuses on the interplay of the phase stiffness and the proximity effect in the framework of a transparent single-vortex picture of the BKT transition, leaving aside a possibility of interface superconductivity and the effect of multivortex correlations on T_b.

The paper is organized as follows. In Sec. II, the BKT transition in a dirty film is discussed, taking into account the effect of subgap states on T_b. In Sec. III, restoration of the mean-field T_c in solid and granular films covered with a high-T_c overlayer is considered. Section IV is devoted to the calculation of T_c of S-N bilayers, taking into account the contact resistance and subgap states. In Sec. V, reduction of the Ginzburg number and the effect of fluctuations on the transition temperature in a bilayer is addressed. In Sec. VI, a nonmonotonic dependence of the BKT transition temperature $T_b(d_2)$ on the thickness of a conductive N overlayer is calculated. In Sec. VII, finite-size effects in the resistive transition caused by thermally activated hopping of complete and fractional vortices in bilayers are considered. In Sec. VIII, broader implications of the obtained results for the reduction of fluctuations in 2D superconductors are discussed.

II. BKT TRANSITION IN A THIN FILM

This section gives a brief overview of the BKT transition temperature T_b in dirty s-wave superconducting films for

which the reduction of T_b relative to the mean-field critical temperature T_c is most pronounced. Hereafter, thin films with the Pearl magnetic penetration depth $\Lambda = \lambda_L^2/d_1$ [45] larger than a lateral film size L are considered, where d_1 is the film thickness and λ_L is the bulk London penetration depth.

A. Nongranular films

The BKT temperature is determined by the energy of a perpendicular vortex $\epsilon = \epsilon_0 \ln(L/\xi)$ in a thin film [18,19]:

$$\zeta \epsilon_0(T_b) = 2T_b. \tag{1}$$

Here the factor $\zeta < 1$ takes into account renormalization of the mean-field superfluid density by fluctuations (hereafter T is measured in energy units). For instance, Monte Carlo simulations of vortices in the XY model [46–48] gave $\zeta = 0.58$. In addition, ζ is reduced by weak-localization effects in disordered films and amplitude fluctuations of the order parameter [49,50].

The energy of the vortex ϵ in a thin film mostly comes from the kinetic energy of circulating currents. In the dirty limit ϵ is given by [51]

$$\epsilon = \int K(\mathbf{r})d^2\mathbf{r} + \epsilon_c, \tag{2}$$

$$K(\mathbf{r}) = \frac{\pi \hbar \sigma_1 d_1 T}{2e^2} Q^2(\mathbf{r}) \sum_{\omega>0} \frac{\Delta^2}{\omega^2 + \Delta^2}, \tag{3}$$

where $\mathbf{Q} = \nabla \chi + 2\pi \mathbf{A}/\phi_0$ is proportional to the superfluid velocity, χ is the phase of the order parameter, $\mathbf{A}$ is the vector potential, σ_1 is a normal-state conductivity, ϕ_0 is the flux quantum, e is the electron charge, $\epsilon_c \simeq 0.5\epsilon_0$ is a vortex core energy [52], and Δ is the superconducting gap. Summing up over the Matsubara frequencies $\omega = \pi T(2n + 1)$ and integrating in Eq. (2) with $Q = 1/r$ for a film with $\Lambda > L$ gives $\epsilon = \epsilon_0 \ln(L/\xi) + \epsilon_c$, where

$$\epsilon_0 = \frac{\pi \Delta R_0}{8R} \tanh \frac{\Delta}{2T}, \quad R_0 = \frac{h}{e^2}. \tag{4}$$

Here $R = (d_1\sigma_1)^{-1}$ is the sheet film resistance in the normal state, and $R_0 = 25.8$ kΩ. Equations (1) and (4) combined with the BCS gap equation for $\Delta(T)$ form the basis for the calculations of T_b in dirty films [53].

This conventional approach does not take into account the essential effects of weak localization [49], inhomogeneities [54,55], and grain boundaries in polycrystalline films on T_b. Another relevant materials feature is the broadening of the gap singularities in the BCS density of states (DOS) $N(\epsilon)$. Numerous STM experiments have shown that the DOS broadening can be significant, particularly in thin films and bilayers [33,56–59]. This effect is usually taken into account in the Dynes model [60,61]:

$$N(\epsilon) = \text{Re} \frac{N_1(\epsilon + i\Gamma)}{\sqrt{(\epsilon + i\Gamma)^2 - \Delta^2}}, \quad \epsilon > 0. \tag{5}$$

Here Γ quantifies a finite lifetime of quasiparticles $\sim \hbar/\Gamma$ resulting in subgap states at $\epsilon < \Delta$, and N_1 is the density of states in the normal state. Many mechanisms of subgap states have been considered in the literature, including inelastic scattering of quasiparticles on phonons [51,62], Coulomb correlations

[63], anisotropy of the Fermi surface [64], inhomogeneities of the BCS pairing constant [65], magnetic impurities [66], spatial correlations in impurity scattering [66,67], or diffusive surface scattering [68].

The phenomenological Eq. (5) captures the broadening of the DOS peaks at $\epsilon \approx \Delta$, but it does not correctly describe low-energy tails in $N(\epsilon)$ obtained in microscopic calculations (see, e.g., Ref. [69] for an overview of different mechanisms). Details of exponential or power-law energy tails in $N(\epsilon)$ at $|\epsilon| \ll \Delta$ can be essential for the calculations of residual quasi-particle conductivity and surface resistance [70]. However, vortex effects considered here are determined by the superfluid density, which is weakly affected by the low-energy tails of $N(\epsilon)$ at $\epsilon \ll \Delta$. Thus, the conventional Eq. (5) in which all microscopic mechanisms are included in a single parameter Γ is rather useful to address the effect of the DOS broadening on the BKT transition by the simple substitution $\omega \to \omega + \Gamma$ in Eqs. (2) and (3). In this approach, Γ is regarded as a material parameter, which can be extracted from tunneling measurements. Then Eqs. (3) and (4) yield

$$\epsilon_0 = \frac{\Delta R_0}{4R} \text{Im}\,\psi\left[\frac{1}{2} + \frac{\Gamma}{2\pi T} + \frac{i\Delta}{2\pi T}\right], \qquad (6)$$

where $\psi(z)$ is a digamma function. At $\Gamma = 0$, Eq. (6) reduces to Eq. (4) since $\text{Im}\,\psi(1/2 + ix) = (\pi/2)\tanh(\pi x)$. The equation for the pair potential Δ is given by

$$\ln\frac{T_c}{T} = \sum_{n=0}^{\infty}\left[\frac{1}{n_1 + \gamma} - \frac{1}{\sqrt{(n_1 + \gamma)^2 + (\Delta/2\pi T)^2}}\right], \quad (7)$$

where $n_1 = n + 1/2$ and $\gamma = \Gamma/2\pi T$. The critical temperature is determined by the equation similar to that describing the reduction of T_c by magnetic impurities [66]:

$$\ln\frac{T_{c1}}{T_c} = U\left(\frac{\Gamma}{2\pi T_c}\right), \qquad (8)$$

$$U(x) = \psi\left(\frac{1}{2} + x\right) - \psi\left(\frac{1}{2}\right), \qquad (9)$$

where $T_{c1} = (2\gamma_E \Omega_1/\pi)\exp(-1/\lambda_1)$, λ_1 is a BCS pairing constant, Ω_1 is the Debye frequency, and $\gamma_E = 1.78$. Here T_c vanishes at $\Gamma > \pi T_{c1}/\gamma_E$ and decreases linearly with Γ at $\Gamma \ll 2\pi T_{c1}$:

$$T_c = T_{c1} - \frac{\pi\Gamma}{4}. \qquad (10)$$

This equation may describe the reduction of T_c in thin films due to the DOS broadening as the film thickness decreases, consistent with tunneling measurements [33,57–59].

Combining Eqs. (1) and (6) yields the following equation for the BKT temperature $T_b(R)$:

$$\frac{R}{R_0} = \frac{\zeta\Delta}{8T_b}\text{Im}\,\psi\left[\frac{1}{2} + \frac{\Gamma}{2\pi T_b} + \frac{i\Delta}{2\pi T_b}\right]. \qquad (11)$$

Shown in Fig. 1 is $T_b(R)$ calculated from Eqs. (7), (8), and (11) for different values of the DOS broadening parameter $\gamma_1 =$
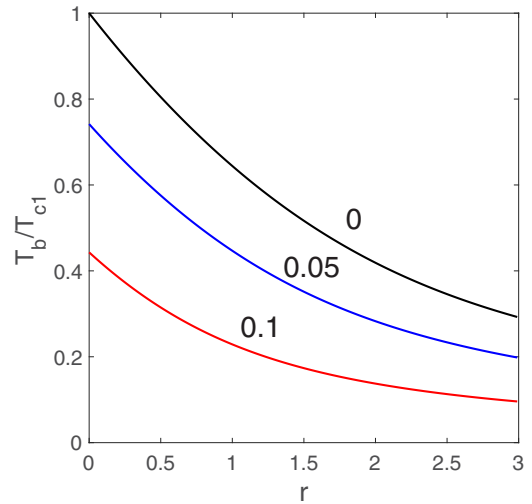

FIG. 1. The BKT transition temperature as a function of the resistance ratio $r = 8R/\pi\zeta R_0$ at different values of the DOS broadening parameter $\Gamma/2\pi T_{c1}$ calculated from Eq. (11).

$\Gamma/2\pi T_{c1}$. Here the DOS broadening reduces the magnitudes of T_c and T_b, but the overall dependence of the normalized T_b/T_c on the sheet resistance does not change qualitatively as Γ increases.

B. Granular films and Josephson junction arrays

Granular films and Josephson junction arrays can be modeled by the energy functional of the XY model [71,72],

$$F = E_J \sum_{i \neq j}[1 - \cos(\chi_i - \chi_j)], \qquad (12)$$

where the coupling energy $E_J = \hbar I_c/2e$ is proportional to the intergrain Josephson critical current I_c, and χ_j is the phase in the jth grain. The energy of a vortex is then $\epsilon = \pi E_J \ln(L/a)$, where a is a grain size. For SIS junctions, $I_c = (\pi\Delta/2eR_i)\tanh(\Delta/2T)$ is inversely proportional to the tunneling contact resistance R_i between the grains [73], so that $\pi E_J = (\pi\Delta R_0/8R_i)\tanh(\Delta/2T)$. For identical grain contacts, the equation for the BKT temperature $2T_b = \zeta\pi E_J$ thus becomes

$$\frac{R_i}{R_0} = \frac{\pi\zeta\Delta}{16T_b}\tanh\frac{\Delta}{2T_b}, \qquad (13)$$

where $\Delta(T_b)$ is determined by Eqs. (7) and (8), and the factor $\zeta < 1$ takes into account mechanisms that reduce I_c as compared to the BCS model, including fluctuations [72] and material factors, which can result in $\zeta \simeq 0.2$–0.8 [73]. Equation (13) coincides with Eq. (11) at $\Gamma = 0$ for a nongranular film with the replacement $R_i \to R$.

For large R_i, the film sheet resistance $R = \alpha_i \bar{R}_i$ is proportional to a mean value $\bar{R}_i$, where the geometric constant α_i depends on the spatial distribution of intergrain contacts, grain shapes, and distribution functions of intergrain areas A_i and critical current densities [74,75]. The relations $R \propto \bar{R}_i$ and $\epsilon \propto R^{-1}$ no longer hold if the intergrain contacts are SNS Josephson junctions for which the $I_c R_i$ product can be much smaller than for SIS junctions [25,26]. Here the energy of the
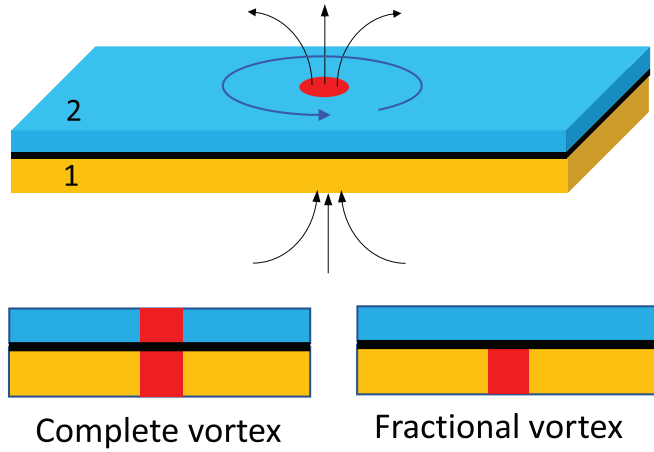
FIG. 2. A perpendicular vortex in a superconducting bilayer. The horizontal black line represents either a weakly coupled planar Josephson junction or an interface with a sheet contact resistance R_B. The bottom panel shows a complete core of a single-quantized vortex in a phase-locked bilayer (left) and a partial core of a fractional vortex (right).

vortex $\epsilon_J = \pi \hbar I_c / 2e$ and the BKT temperature can be greatly reduced by weakly coupled SNS grain boundaries, which do not necessarily result in high sheet resistance.

III. WEAKLY COUPLED OVERLAYER

Consider two superconducting layers separated by a planar Josephson junction with the critical current density J_c, as shown in Fig. 2. Let the layers 1 and 2 have the critical temperature T_{c1} and $T_{c2} > T_{c1}$, and the gaps Δ_1 and Δ_2 be unaffected by weak Josephson coupling. The energy of a perpendicular vortex depends crucially on whether both layers are in a phase-locked state with $\chi_1(\mathbf{r}) = \chi_2(\mathbf{r})$ or in a phase-unlocked state with different phases of the order parameter $\chi_1(\mathbf{r})$ and $\chi_2(\mathbf{r})$ in the layers 1 and 2. In the first case, the vortex core threads both layers, which thus have the same distribution of $Q(r)$. In a phase-unlocked bilayer, a fractional vortex with a partial vortex core that threads only a lower-T_c layer 1 can occur. The fractional vortex has a smaller kinetic energy of supercurrents in the layer 2, but it produces the interlayer phase difference, $\chi = \chi_2 - \chi_1$, and thus the Josephson energy $W_J = (\hbar J_c / 2e) \int (1 - \cos \chi) dx \, dy \sim \hbar J_c L w / 2e$ proportional to the area of the bilayer of length L and width w, as shown in Appendix C. For instance, if T_{c1} and T_{c2} are not very different, $J_c = \pi \Delta_1 \Delta_2 / 4e R_\perp T_{c1}$ at $T \approx T_{c1}$, where $R_\perp$ is the interface resistance per unit area [26]. The energy difference ΔW between the partial and the complete vortex is then

$$\Delta W \simeq \frac{\Delta_1 \Delta_2 R_0}{16 T_{c1} R_\perp} L w - \frac{\pi \Delta_2^2 R_0}{16 T_{c2} R_2} \ln \frac{w}{\xi_2}, \qquad (14)$$

where $R_2 = (d_2 \sigma_2)^{-1}$ is the sheet resistance of layer 2. The first term in Eq. (14) describes the loss of the Josephson energy in a phase-unlocked bilayer, and the second term is the gain in the kinetic energy in the layer 2. The complete vortex is more energetically favorable in wide films or long bridges in which

$\Delta W > 0$ and

$$L > L_c \simeq (\pi R_\perp \Delta_2 / w \Delta_1 R_2) \ln(w / \xi_2). \qquad (15)$$

Fractional vortices may occur in narrow short bridges with $L < L_c$, particularly at $T \to T_{c1}$ where $\Delta_1(T)/\Delta_2 \lesssim (R_\perp / R_2 L w) \ln(w/\xi)$. Here we focus on the BKT transition due to proliferation of complete vortices.

The energy of a complete vortex is a sum of kinetic energies of currents in the layers 1 and 2 given by Eq. (4) for negligible DOS broadening. In this case, the equation for the BKT temperature takes the form

$$\frac{R_1}{R_0} = \frac{\pi \zeta}{16 T_b} \left[\Delta_1 \tanh \frac{\Delta_1}{2 T_b} + \frac{d_2 \sigma_2}{d_1 \sigma_1} \Delta_2 \tanh \frac{\Delta_2}{2 T_b} \right]. \qquad (16)$$

As the overlayer thickness d_2 increases, T_b increases and exceeds T_{c1} of the layer 1 if

$$d_2 > d_{2c} = \frac{16 T_{c1}}{\pi \zeta \Delta_2(T_{c1}) \sigma_2 R_0} \coth \frac{\Delta_2(T_{c1})}{2 T_{c1}}, \qquad (17)$$

where $\Delta_1(T_b) = 0$. As d_2 approaches d_{2c}, the fractional vortex becomes more energetically favorable. Yet the high-T_c overlayer restores the mean field T_{c1} in the layer 1 by increasing the sheet superfluid density and suppressing the BKT proliferation of vortices.

IV. PROXIMITY-COUPLED OVERLAYER

In this section, we follow the well-established theory of T_c in a dirty thin-film bilayer [25–29] and take into account the effect of the DOS broadening essential in the subsequent analysis. A dirty bilayer comprising a superconductor 1 at $-d_1 < x < 0$ and a superconductor 2 at $0 < x < d_2$ can be described by the Usadel equations:

$$-D_1 \theta_1'' + 2\omega \sin \theta_1 = 2\Delta_1 \cos \theta_1, \qquad (18)$$

$$-D_2 \theta_2'' + 2\omega \sin \theta_2 = 2\Delta_2 \cos \theta_2, \qquad (19)$$

where D_1 and D_2 are electron diffusivities in the layers 1 and 2, respectively, and

$$\Delta_{1,2} = 2\pi T \lambda_{1,2} \sum_{\omega > 0}^{\Omega_{1,2}} \sin \theta_{1,2}. \qquad (20)$$

Here (λ_1, Ω_1) and (λ_2, Ω_2) are the pairing constant and the Debye frequency in a superconductor 1 and 2, respectively. Equations (18) and (19) are supplemented by the boundary conditions [26]

$$\sigma_2 \theta_2'(0) = \sigma_1 \theta_1'(0) = R_B^{-1} \sin(\theta_1 - \theta_2), \qquad (21)$$

$$\theta_1'(-d_1) = \theta_2'(d_2) = 0, \qquad (22)$$

where R_B is the sheet contact resistance of the interface. The DOS broadening is taken into account by $\omega \to \omega_1 = \omega + \Gamma_1$ in Eq. (18) and $\omega \to \omega_2 = \omega + \Gamma_2$ in Eq. (19).

In this paper, a thin-film Cooper limit is considered in which $d_{1,2} \ll (\hbar D_{1,2} / 2\pi T_c)^{1/2}$ so that $\theta_1(x)$ and $\theta_2(x)$ are nearly constant across the layers [24]. In this case, the solution of Eqs. (18) and (19) given in Appendix A yields two coupled

equations for θ_1 and θ_2:

$$\tan\theta_2 = \frac{\sin\theta_1 + \alpha\beta\Delta_2}{\cos\theta_1 + \alpha\beta\omega_2}, \tag{23}$$

$$\Delta_1\cos\theta_1 - \omega_1\sin\theta_1$$
$$= \frac{\alpha(\omega_2\sin\theta_1 - \Delta_2\cos\theta_1)}{\sqrt{1 + \alpha^2\beta^2(\omega_2^2 + \Delta_2^2) + 2\alpha\beta(\omega_2\cos\theta_1 + \Delta_2\sin\theta_1)}}, \tag{24}$$

$$\alpha = \frac{d_2 N_2}{d_1 N_1}, \quad \beta = 4d_1 N_1 e^2 R_B. \tag{25}$$

General solutions of Eqs. (20), (23), and (24) can be obtained numerically. For a negligible contact resistance, $\alpha\beta\Omega_{1,2} \ll 1$, Eqs. (23) and (24) yield $\theta_1 = \theta_2 \equiv \theta$, and the bilayer is described by the composite parameters:

$$\sin\theta = \frac{\Delta}{\sqrt{(\omega + \Gamma)^2 + \Delta^2}}, \tag{26}$$

$$\Delta = \frac{d_1 N_1 \Delta_1 + d_2 N_2 \Delta_2}{d_1 N_1 + d_2 N_2}, \tag{27}$$

$$\Gamma = \frac{d_1 N_1 \Gamma_1 + d_2 N_2 \Gamma_2}{d_1 N_1 + d_2 N_2}. \tag{28}$$

The critical temperature T_{c0} of the bilayer is obtained by linearizing Eqs. (18)–(20) with respect to $\theta_{1,2} \ll 1$:

$$T_{c0} = T_{c1} \exp\left[\frac{\alpha[\lambda_2 - \lambda_1 + \lambda_1\lambda_2\ln(\Omega_2/\Omega_1)]}{(\lambda_1 + \alpha\lambda_2)\lambda_1}\right], \tag{29}$$

where $T_{c1} = (2\gamma_E\Omega_1/\pi)\exp(-1/\lambda_1)$ is the critical temperature of the superconductor 1 with $\lambda_1 > \lambda_2$. The equation for T_c in a bilayer with $\Gamma > 0$ and $R_B = 0$ reduces to Eq. (8) in which $T_{c1} \to T_{c0}$, and Γ and T_{c0} are given by Eqs. (28) and (29).

A general equation for T_c at arbitrary R_B was obtained in Appendix A. For a bilayer comprising a normal overlayer with $\lambda_2 = 0$, this equation simplifies to

$$\frac{1}{\lambda_1} = 2\pi T_c \sum_{\omega>0} \frac{(1 + \alpha\beta\omega_2)}{[\omega_1(1 + \alpha\beta\omega_2) + \alpha\omega_2]} \frac{\Omega_1^2}{(\omega^2 + \Omega_1^2)}. \tag{30}$$

Here the ad hoc factor $\Omega_1^2/(\omega^2 + \Omega_1^2)$ provides convergence of the sum for any relation between $\alpha\beta$ and Ω_1, reproducing the BCS results while eliminating artifacts coming from the hard cutoffs in the sums at $\omega = \Omega_1$ in realistic cases of not very large $\Omega_1/2\pi T_c$. If Γ_1 and Γ_2 are negligible, Eq. (30) becomes (see Appendix A)

$$\ln\frac{T_c}{T_{c0}} = \frac{\alpha(\alpha\beta\Omega_1)^2}{(\alpha\beta\Omega_1)^2 + (1 + \alpha)^2}\left[\ln\frac{2\gamma_E\Omega_1}{\pi T_c}\right.$$
$$\left. + \frac{\pi(1 + \alpha)}{2\alpha\beta\Omega_1} - U\left(\frac{1 + \alpha}{2\pi\alpha\beta T_c}\right)\right], \tag{31}$$

where $T_{c0} = T_{c1}\exp(-\alpha/\lambda_1)$ is the critical temperature of the bilayer with $\beta \propto R_B = 0$. The contact resistance weakens the proximity effect coupling of the S and N layers, ameliorating the decrease of T_c with d_2, as shown in Fig. 3. The strongest proximity effect suppression of T_c described by Eq. (29) occurs at $R_B = 0$. At nonzero contact resistance, $T_{c0}(d_2)$ does not

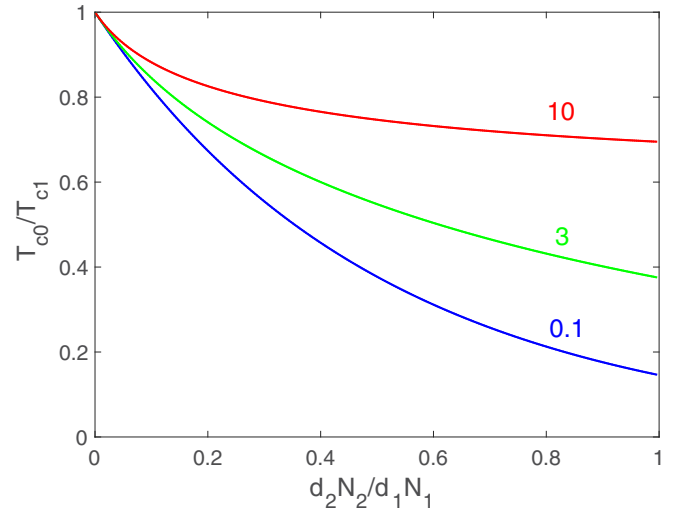FIG. 3. Critical temperature $T_{c0}(d_2)$ of the N-S bilayer calculated from Eq. (31) for $\lambda_1 = 0.5$, $\lambda_2 = 0$, and different values of the contact resistance parameter $2\pi\beta T_{c1} = 0.1, 3, 10$.

vanish at $d_2 \to \infty$ but approaches a minimum value $T_{\min}$, which increases with R_B so that $T_{\min} \to T_{c1}$ at $\alpha\beta\Omega_1 \gg 1$.

Figure 4 shows the effect of DOS broadening on $T_c(d_2)$ in an N-S bilayer with $R_B = 0$ and $\lambda_2 = 0$ calculated from Eqs. (8) and (9) for different values of $\gamma_1 = \Gamma/2\pi T_{c1}$. Here the DOS broadening causes a steeper decrease of T_c with d_2, and the critical temperature vanishes if $d_2 > d_c$. Setting $T_c \to 0$ and using $\psi(z) = \ln z$ at $z \gg 1$ in Eqs. (8) and (9) yields the following equation for d_c:

$$\Gamma(d_c) = \pi T_{c0}(d_c)/\gamma_E, \tag{32}$$

which has the same form as the equation for the critical concentration of paramagnetic impurities in the Abrikosov-Gorkov theory [66].

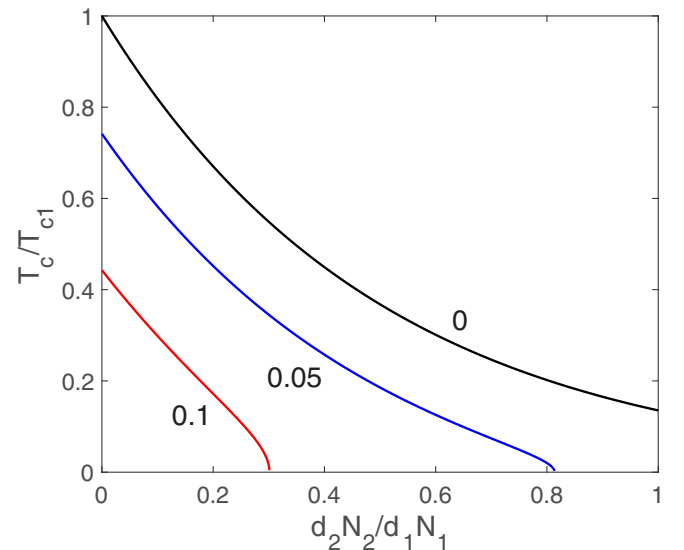FIG. 4. Critical temperature $T_c(d_2)$ of the N-S bilayer calculated from Eqs. (8), (9), (28), and (29) for $\lambda_1 = 0.5$, $\lambda_2 = 0$, and different values of $\gamma_1 = \Gamma/2\pi T_{c1}$.

V. FLUCTUATIONS IN N-S BILAYERS

For a phase-locked N-S bilayer with $R_B = 0$, the Ginzburg-Landau (GL) free-energy functional is given by (see Appendix B)

$$F = \int \left[a(T)|\Psi|^2 + c \left| \left(\nabla - \frac{2\pi i \mathbf{A}}{\phi_0} \right) \Psi \right|^2 + \frac{b}{2}|\Psi|^4 \right] d^2\mathbf{r}, \tag{33}$$

$$a = \frac{(T_{c0} - T)\nu}{T_{c0}}, \quad b = \frac{7\zeta(3)\nu}{8\pi^2 T_{c0}^2}, \tag{34}$$

$$c = \frac{\pi \hbar}{8 T_{c0}}(d_1 N_1 D_1 + d_2 N_2 D_2), \tag{35}$$

where $\Psi = \Delta e^{i\chi}$ is the order parameter. The mean-field jump in the specific heat $\Delta C = \nu^2 / b T_{c0}$ at T_{c0} is then

$$\Delta C = \frac{8\pi^2 \nu T_{c0}}{7\zeta(3)}, \quad \nu = d_1 N_1 + d_2 N_2. \tag{36}$$

The Gaussian fluctuation correction to the sheet specific heat [76] is readily obtained from Eq. (33):

$$\delta C(T) = \frac{2\nu e^2 T_{c0}^2}{\pi^2 \hbar (d_1 \sigma_1 + d_2 \sigma_2)(T_{c0} - T)}, \quad T > T_{c0}. \tag{37}$$

The width of the critical region of strong fluctuations $T_f - T_{c0}$, where $\delta C(T_f) = \Delta C$ defines the Ginzburg parameter $\mathrm{Gi} = (T_f - T_{c0})/T_{c0}$ given by:

$$\mathrm{Gi} = \frac{7\zeta(3)e^2}{4\pi^4 \hbar (d_1 \sigma_1 + d_2 \sigma_2)} = \frac{7\zeta(3)R_\square}{2\pi^3 R_0}. \tag{38}$$

Here Gi, controlled by the ratio of the bilayer normal sheet resistance $R_\square = (d_1 \sigma_1 + d_2 \sigma_2)^{-1}$ and the quantum resistance $R_0 = h/e^2$, does not depend on superconducting properties [76]. A thin overlayer with $\sigma_2 \gg \sigma_1$ and $d_2 > d_1 \sigma_1 / \sigma_2 \ll d_1$ can thus strongly reduce Gi and mitigate fluctuations without a significant suppression of T_{c0} due to the proximity effect.

The GL coherence length ξ is defined here by the condition $a\Delta^2 \simeq c\Delta^2/\xi^2$, giving

$$\xi = \left[\frac{\pi \hbar (d_1 \sigma_1 + d_2 \sigma_2)}{16 \nu e^2 |T_{c0} - T|} \right]^{1/2}. \tag{39}$$

Generally, the global phase coherence is lost at a transition temperature $\tilde{T}_c$ at which the thermal energy T is of the order of the condensation energy $\pi a^2 \xi^2/2b$ within a correlated area $\pi \xi^2$, that is, $\mu_1 \tilde{T}_c = a^2(\tilde{T}_c)\pi \xi^2(\tilde{T}_c)/2b$, where $\mu_1 \sim 1$. Using Eqs. (34) and (39) here yields

$$\tilde{T}_c = \frac{T_{c0}(d_2)}{1 + \mu R_\square(d_2)/R_0}, \tag{40}$$

where $\mu = 56\zeta(3)\mu_1/\pi^3$. For instance, the BKT transition corresponds to $\mu_1 \simeq 1/2$ and $\mu \simeq 1.1$. Fluctuations reduce $\tilde{T}_c$ relative to T_{c0}, but as the overlayer thickness increases, the effect of fluctuations weakens while $T_{c0}(d_2)$ gets diminished by the proximity effect. If $\sigma_2 \gg \sigma_1$, the transition temperature $\tilde{T}_c(d_2)$ first increases with d_2 due to decreasing $R_\square(d_2)$ in Eq. (40) and then decreases at larger d_2 as the proximity effect takes over. The nonmonotonic $\tilde{T}_c(d_2)$ occurs if $\partial \tilde{T}_c / \partial d_2 > 0$ at

$d_2 \to 0$, which in the case of $R_B = 0$ and $\lambda_2 = 0$ reduces to

$$\frac{D_2}{D_1} > \frac{1}{\lambda_1}\left(1 + \frac{R_0}{\mu R}\right). \tag{41}$$

This inequality can be satisfied for a highly conductive N overlayer with $q = D_2/D_1 \gg 1$. Here the maximum $\tilde{T}_c$ defined by Eqs. (29) and (40) occurs at $\alpha_m = (\mu R/R_0 \lambda_1 q)^{1/2} \ll 1$, and the optimum overlayer thickness d_{2m} and the transition temperature $\tilde{T}_c(d_{2m}) = T_{c1}(1 - 2\alpha_m/\lambda_1)$ become

$$d_{2m} = \frac{d_1 N_1}{N_2}\left(\frac{\mu \lambda_1 R}{R_0 q} \right)^{1/2}, \tag{42}$$

$$\tilde{T}_c(d_{2m}) = T_{c1}\left(1 - 2\sqrt{\frac{\mu R}{\lambda_1 q R_0}} \right). \tag{43}$$

At $q = D_2/D_1 \ll 1$, the optimum overlayer thickness d_{2m} is much smaller than the thickness of the S film, neither d_{2m} nor $\tilde{T}_c(d_{2m})$ depending on D_1. Such an N overlayer can nearly restore $\tilde{T}_c$ to the mean-field T_{c1} of the S film. Equations (33)–(35) do not take into account renormalization of the GL coefficients due to strong electron-pnonon coupling [77–79], and weak-localization effects, which become essential for large R [49]. These effects influence the numerical factor μ but do not change the conclusion that a thin, highly conductive overlayer mitigates superconducting fluctuations.

VI. BKT TRANSITION IN A BILAYER

The interplay of the proximity effect and the phase stiffness manifests itself in the BKT transition temperature, which shows how T_r is affected by a thin overlayer. Here the vortex energy scale ϵ_0 in Eq. (1) is determined by the sum of kinetic energies of circulating currents in the phase-locked layers 1 and 2:

$$\epsilon_0 = \frac{\pi^2 \hbar T}{e^2} \sum_{\omega > 0} [d_1 \sigma_1 \sin^2 \theta_1 + d_2 \sigma_2 \sin^2 \theta_2]. \tag{44}$$

Calculation of $T_b(\alpha)$ in the general case when R_B is essential requires numerical solution of coupled Eqs. (1), (23), (24), and (44). The behavior of $T_b(\alpha)$ becomes more transparent in a bilayer with a negligible R_B for which the enhancement of the phase stiffness by the overlayer is most pronounced. In this case, $\theta_1 = \theta_2 \equiv \theta$ is given by Eq. (26), and Eq. (44) becomes

$$\epsilon_0 = \frac{\pi R_0}{2R}(1 + q\alpha)S, \quad q = \frac{D_2}{D_1}, \tag{45}$$

$$S = T\sum_{\omega > 0} \sin^2 \theta = \frac{\Delta}{2\pi} \mathrm{Im}\psi\left[\frac{1}{2} + \gamma + \frac{i\Delta}{2\pi T} \right]. \tag{46}$$

Here $\gamma = \Gamma/2\pi T$ and $S = (\Delta/4)\tanh(\Delta/2T)$ at $\gamma = 0$. The vortex core radius $\simeq \xi$ given by Eq. (39) can be significantly increased by a highly conductive overlayer.

Using Eqs. (1) and (45), the equation for the BKT temperature T_b can be written in the form

$$\frac{R}{R_0} = \frac{\zeta\Delta}{8T_b}(1 + q\alpha)\mathrm{Im}\psi\left[\frac{1}{2} + \frac{\Gamma}{2\pi T_b} + \frac{i\Delta}{2\pi T_b} \right]. \tag{47}$$

Here T_b and the composite gap parameter Δ as functions of the film sheet resistance $R = (\sigma_1 d_1)^{-1}$ and the overlayer thickness are determined self-consistently by Eqs. (7), (27),

(28), and (47). The factor ζ accounts for the renormalization of the superfluid density and diffusivities due to strong electron-phonon coupling [77–79], fluctuations and weak-localization effects [49]. Given the complexity of the theoretical account of these mechanisms in bilayers affected by many uncertain microscopic parameters, ζ is treated here as a material parameter that can be expressed in terms of the observed T_b in a single S film [80].

If $\Gamma = 0$, the equations for T_b can be written in the convenient parametric form:

$$q\alpha = \frac{r}{p}\coth p - 1, \qquad r = \frac{8R}{\pi \zeta R_0}, \qquad (48)$$

$$\ln\frac{T_{c1}}{T_b} - \frac{\alpha[\lambda_1 - \lambda_2 - \lambda_1\lambda_2\ln(\Omega_2/\Omega_1)]}{(\lambda_1 + \alpha\lambda_2)\lambda_1}$$

$$= \sum_{n=0}^{\infty}\left[\frac{1}{n+\frac{1}{2}} - \frac{1}{\sqrt{\left(n+\frac{1}{2}\right)^2 + (p/\pi)^2}}\right]. \qquad (49)$$

Shown in Fig. 5 is $T_b(\alpha)$ calculated from Eqs. (48) and (49) for different resistance parameters r as the parameter $p = \Delta/2T_b$ increases from 0 to ∞. The behavior of $T_b(\alpha)$ depends essentially on the diffusivity ratio $q = D_2/D_1$. At $q \lesssim 1$, both $T_{c0}(\alpha)$ and $T_b(\alpha)$ decrease with the overlayer thickness in a way expected from the proximity effect, the difference between $T_b(\alpha)$ and $T_{c0}(\alpha)$ increasing with r. However, if $q \gg 1$, the BKT temperature $T_b(\alpha)$ first increases with d_2, reaching a maximum at $d_2 \ll d_1$, and then approaches $T_{c0}(\alpha)$ at larger d_2 as shown in Fig. 5(b). This nonmonotonic $T_b(\alpha)$ at $q \gg 1$ results from the interplay of the increasing sheet superfluid density and the decreasing T_{c0} due to the proximity effect, as was discussed in the previous section.

The DOS broadening reduces both T_{c0} and the BKT transition temperature. For a single film, the DOS broadening does not change qualitatively the dependence of T_b on r except for the overall reduction of $T_b(r)$ as shown in Fig. 1. The effect of DOS broadening on the nonmonotonic dependence of $T_b(\alpha)$ in a bilayer with $R_B = 0$ and $D_2 \gg D_1$ is shown in Fig. 6, where $T_b(\alpha)$ was calculated from Eqs. (27), (7), and (47). Here $T_b(\alpha)$ also decreases as the broadening parameter $\Gamma/2\pi T_{c1}$ increases. This may be relevant to experiments [61] in which a nonmonotonic resistive transition temperature as a function of the overlayer thickness in Pb films was observed along with a reduction of T_c and the DOS broadening.

As the contact resistance increases, the proximity-effect suppression of T_{c0} diminishes. At the same time, a significant R_B with $\beta \gtrsim 1$ tends to decouple the layers 1 and 2, suppressing the increase of the phase stiffness by the overlayer. The effect of these opposite trends on T_b can be calculated by solving Eqs. (1), (23), (24), and (44) numerically. At $\beta \gg 1$, the superfluid density caused by the proximity effect in the N overlayer is strongly reduced, and T_b of a bilayer becomes limited by the induced weak superconductivity in the N layer, even if $\sigma_2 \gg \sigma_1$.

VII. FINITE-SIZE EFFECTS

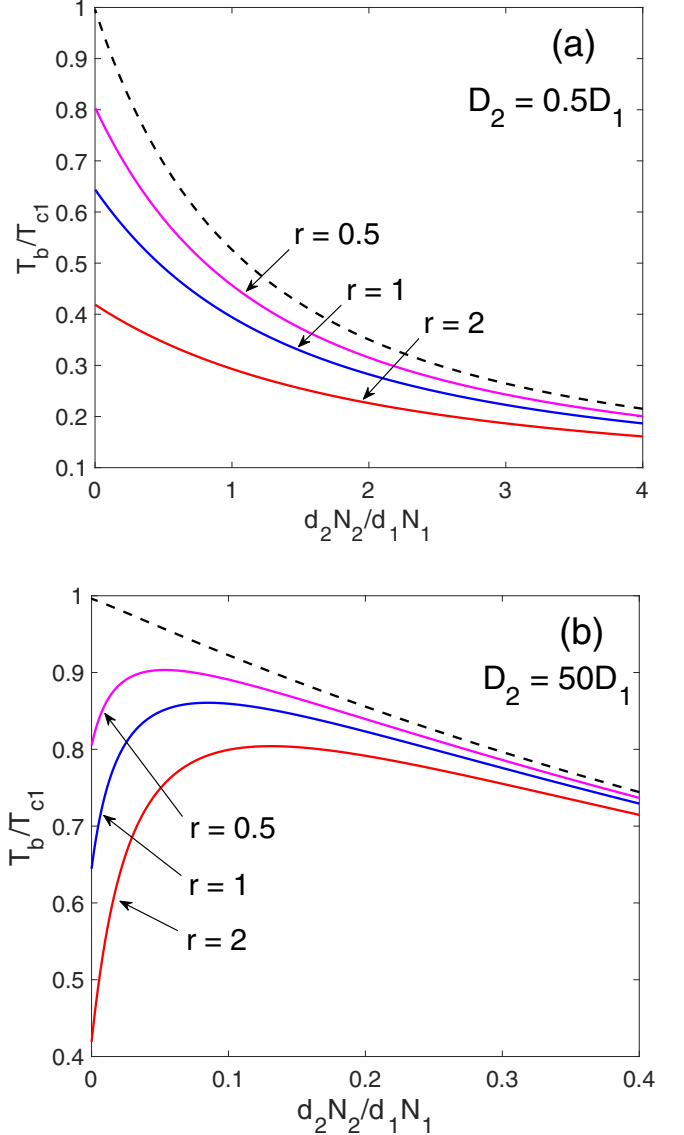Finite-size effects can be essential in thin-film bridges where, in addition to the BKT vortex unbinding, the resis-

FIG. 5. BKT transition temperature $T_b(d_2)$ calculated from Eqs. (48) and (49) for different film resistances, $r = 8R/\pi\zeta R_0$, $\lambda_1 = 0.7$, $\lambda_2 = 0.2$, $\Omega_2 = 2\Omega_1$, and (a) $D_2 = 0.5D_1$ and (b) $D_2 = 50D_1$. The dashed line shows the proximity-effect-limited $T_{c0}(d_2)$ in the absence of the BKT fluctuations.

tive transition is affected by thermally activated hopping of single vortices across the bridge and proliferation of fractional vortices in weakly coupled bilayers.

A. Thermally activated vortex hopping

The dynamics of vortex hopping is determined by the local energy $U(u)$ of the vortex as a function of its position u across the bridge. A vortex in a thin-film strip of width $w < \Lambda$ produces circulating superflow with the normal components $Q_x(0, y) = Q_x(w, y)$ vanishing at the edges, and $\mathbf{Q}(x, y)$ decreasing exponentially over the length w/π along the bridge [81,82] (see Appendix C). The energy barrier $U(u)$ in a strongly coupled bilayer can be calculated in the same way as for a single film [83], except that the vortex energy scale ϵ_0 is now determined by the composite parameters defined by Eqs. (26)
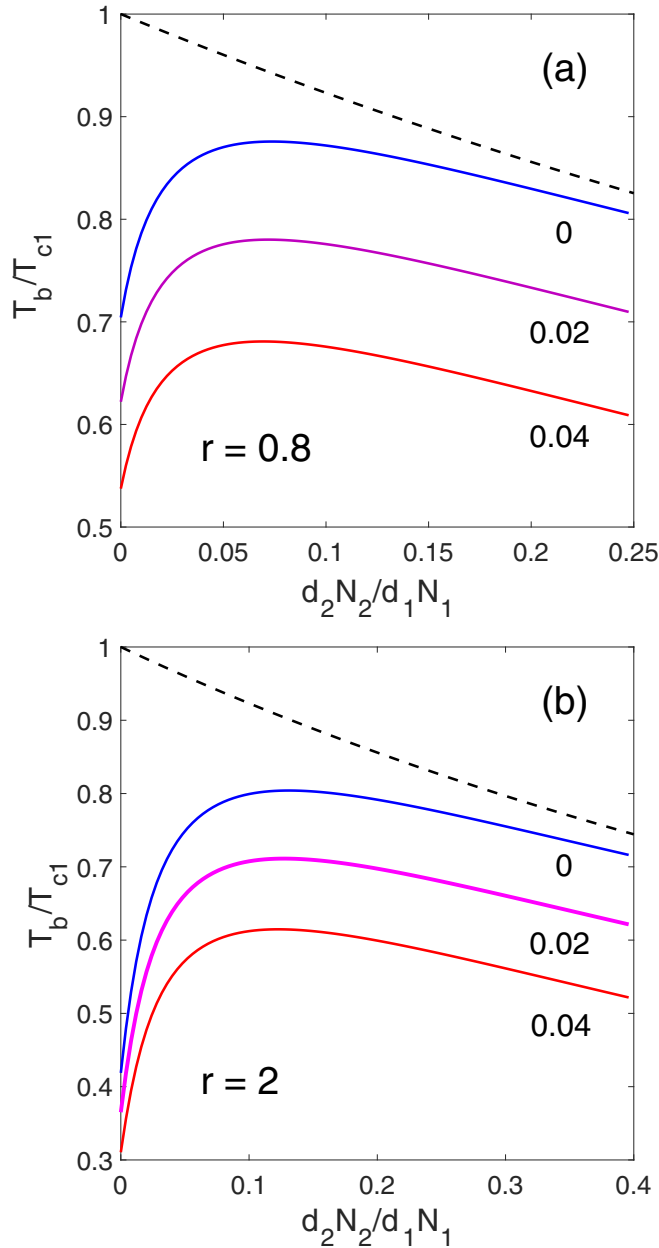
FIG. 6. BKT transition temperature $T_b(d_2)$ calculated from Eqs. (7), (27) and (47) at $D_2 = 50D_1$, $\lambda_1 = 0.7$, $\lambda_2 = 0.2$, and $\Omega_2 = 2\Omega_1$ for different values of the DOS broadening parameter $\Gamma/2\pi T_{c0}$ and the resistance ratios $r = 0.8$ (a) and $r = 2$ (b). The dashed line shows the proximity-effect-limited T_{c0} of the bilayer in the absence of the BKT fluctuations.

and (27):

$$U(u) = \zeta \epsilon_0 \ln[(w/\pi \tilde{\xi}) \sin(\pi u/w)], \qquad (50)$$

where $\tilde{\xi} = C\xi$ is an effective coherence length, and $C \approx 0.34$ accounts for the core energy [83]. The coherence length ξ and the viscous drag coefficient η of a vortex in a bilayer at $T \approx T_c$ were evaluated in Appendix B:

$$\xi = \left[\frac{\pi \hbar D}{8(T_{c0} - T)}\right]^{1/2}, \qquad (51)$$

$$D = \frac{d_1 N_1 D_1 + d_2 N_2 D_2}{d_1 N_1 + d_2 N_2}, \qquad (52)$$

$$\eta = \frac{\phi_0^2}{2\pi \xi^2 R_\square} = 8\hbar(d_1 N_1 + d_2 N_2)(T_{c0} - T). \qquad (53)$$

Here the vortex core size ξ defined by the composite diffusivity D increases as the overlayer thickness increases, but the viscosity η, which takes into account dissipation in the vortex core in both layers, turns out to be independent of σ_1 and σ_2. The latter results from the fact that the diffusivity D cancels out in the product $\xi^2 R_\square$ in Eq. (53), thus η in the Bardeen-Stephen model [51] becomes independent of the mean free paths.

A solution of the Fokker-Planck equation for thermally activated vortex hopping over the barrier $U(x)$ gives the following voltage-current (V-I) characteristics [83]:

$$V = \frac{2\mathcal{R}_n I(z-1)}{s\Gamma(z+1)} \left[\frac{2\pi \tilde{\xi}}{w}\right]^z \left|\Gamma\left(1 + \frac{z}{2} + is\right)\right|^2 \sinh \pi s, \qquad (54)$$

where $\mathcal{R}_n = L/w(d_1\sigma_1 + d_2\sigma_2)$ is the total normal-state resistance, $z = \epsilon_0/T$, $s = \phi_0 I/2\pi T$, and $\Gamma(x)$ is the Gamma function. At small currents, $s \ll 1$, Eq. (54) yields the Ohmic $V = \mathcal{R}I$, where

$$\frac{\mathcal{R}}{\mathcal{R}_n} = \frac{2\pi^{3/2} z \Gamma(z/2)}{\Gamma[(z-1)/2]} \left(\frac{\pi \tilde{\xi}}{w}\right)^z. \qquad (55)$$

These formulas are applicable at $T < T_b$, that is, $z > 2$. If $z \gg 1$, the vortex Ohmic resistance $\mathcal{R} \simeq \sqrt{2}\mathcal{R}_n(\pi z)^{3/2}(\pi \tilde{\xi}/w)^z \ll \mathcal{R}_n$ depends strongly on w. As I increases, the V-I characteristics at $s > 1$ becomes nonlinear, $V \propto I^{z+1}$, and independent of the bridge width [83].

The resistive transition temperature $T_r(I, w)$ calculated from Eqs. (51)–(54) depends not only on the conductivities and thicknesses of the layers but also on the width of the bridge and the electric field or resistance criterion at which T_r is defined in transport measurements. For instance, Fig. 7 shows $T_r(d_2)$ calculated from Eqs. (55) for the resistance criterion $\mathcal{R} = 0.1\mathcal{R}_n$, $w = 10\xi_1$, $D_2 = 100D_1$, and different ratios $r = 8R/\pi \zeta R_0$. Here $z = (2p/r)\tanh p$ depends on the parameter $p = \Delta/2T_r$, which is obtained from Eq. (55) for a particular $\mathcal{R}_v$ and then used to calculate T_r in Eq. (49). The so-obtained dependence $T_r(d_2)$ for a single-vortex hopping appears similar to that of $T_b(d_2)$ calculated in the previous sections, and the nonmonotonic dependence of $T_r(d_2)$ becomes more pronounced if the resistance criterion is chosen at a fixed ratio $\mathcal{R}/R_1$, where $R_1 = L/\sigma_1 d_1 w$.

These calculations of $V(I)$ and T_r were based on Eq. (50) for the energy of a single vortex in a uniform bridge with no material defects in the bulk and perfect film edges. This model is an idealization of a more realistic situation in which a bridge has material defects at the edges and in the bulk, as depicted in Fig. 8. Defects such as nonsuperconducting second phase precipitates, grain boundaries, or variation of the film thickness can pin vortices and lower local activation barriers, resulting in preferential hopping of vortices along chains of defects, as shown in Fig. 8. Such behavior of vortices was recently observed in Pb films by SQUID on tip scanning microscopy [84].
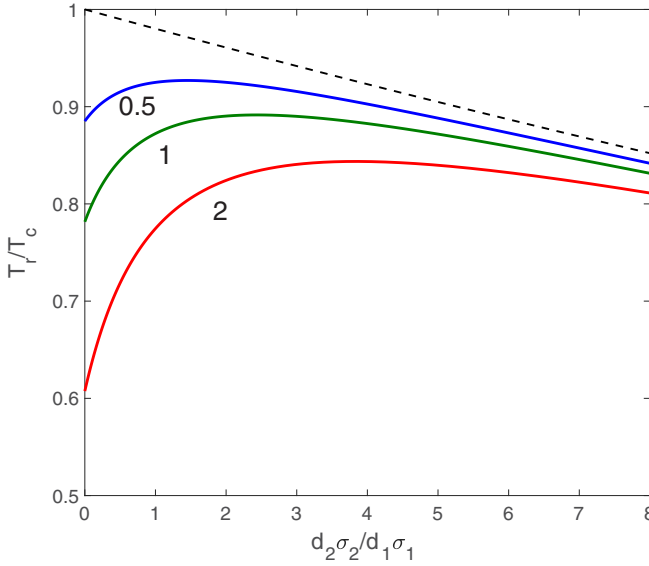
FIG. 7. Temperature of the resistive transition in the NS bilayer as a function of the overlayer thickness calculated from Eqs. (55) at the resistance criterion $\mathcal{R}_v = 0.1\mathcal{R}$, $\lambda_1 = 0.5$, $D_2 = 100 D_1$, $w = 10\xi_1$, and different values of $r = 8R/\pi\zeta R_0$: 0.5, 1, and 2. The dashed line shows the mean-field $T_c(d_2)$.

Pinning centers can facilitate thermally activated vortex hopping and reduce T_r as compared to a uniform bridge. However, a proximity-coupled conductive overlayer can nearly restore T_r back to T_{c0} by increasing the vortex energy scale ϵ_0 and by weakening the effect of the pinning potential on vortex hopping. Indeed, if pinning centers are in the S layer, deposition of the N overlayer would increase ϵ_0 and the vortex energy barriers without affecting the pinning energy. As a result, the nonmonotonic dependence of $T_r(d_2)$ becomes more pronounced because pinning mostly increases the dip in T_r at $d_2 = 0$ while causing only a small correction to T_r at larger d_2 for which the effect of the overlayer becomes dominant.

B. Partial vortices

As was mentioned in Sec. III, partial vortices may occur in a weakly coupled bilayer with small Josephson current density J_c across the interface between the layers 1 and 2. Fractional vortices have been investigated theoretically [85] and observed in bilayers [86]. Partial vortices could contribute to the resistive transition in short bilayer bridges $L < L_c$ at temperatures close to T_{c1} of layer 1 for which the condition (15) is satisfied. In this case, the layers 1 and 2 become phase-unlocked so that the overlayer does not increase the kinetic energy of superflow around a vortex but produces a Josephson energy proportional to the area of the bridge.

The energy of a perpendicular vortex in the granular film 1 can be reduced by weak intergranular contacts, but it does not affect Eq. (15), which defines the condition under which fractional vortices can appear in both granular and nongranular bilayers. The above results are applicable for layers much thinner than the London penetration depth, λ_L, so that the layer 2 is transparent to the magnetic field produced by the vortex in the layer 1. If $d_2 > \lambda_L$, a thick overlayer traps the vortex
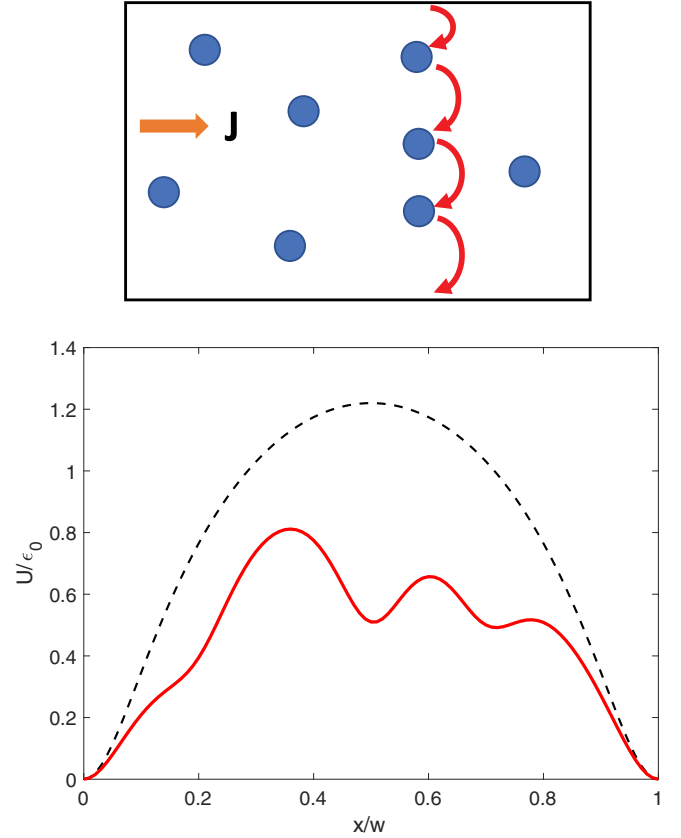

FIG. 8. Top: Thermally activated hopping of the vortex along a chain of pinning centers shown as blue regions. Bottom: Sketch of the local energy of the vortex $U(x)$. The dashed line shows $U(x)$ in a uniform bridge calculated from Eq. (50) at $w = 10\tilde{\xi}$. The solid line shows $U(x)$ given by Eq. (50) plus the pinning potential modeled by three Lorentzian wells, $U_p(x) = -\sum_i U_i \xi^2/[(x - x_i)^2 + \xi^2]$ with $U_i = (0.3, 0.6, 0.4)\epsilon_0$ at $x_i = (0.2, 0.5, 0.7)w$. The London core singularities at $x = 0$ and $x = w$ were regularized to provide zero vortex energy at the edges, $U(0) = U(w) = 0$.

magnetic field and spreads it along the interface between the layers 1 and 2. This increases the magnetic energy of the vortex and the BKT transition temperature [40]. Such an effect would be most pronounced in a thin film sandwiched between two massive superconductors.

A different mechanism of mitigation of vortex fluctuations occurs if a disconnected N overlayer is spaced by a wide gap of width d_i from the superconducting layer 1. It was observed that a 30-nm-thick Au overlayer separated by a 16 nm gap from a 3-nm-thick MoGe film slightly increases the temperature of the resistive transition [37]. This effect was associated with additional dissipation caused by eddy currents induced by a moving vortex in the metallic overlayer, mitigating quantum tunneling of vortices [39]. Here we consider the influence of a remote N overlayer on thermally activating hopping of vortices. This process is controlled by the vortex drag coefficient η, which was calculated in Appendix D:

$$\eta = \frac{\phi_0^2 d_1}{2\pi \xi_1^2 \rho_1} + \frac{(\ln 4 - 1)\phi_0^2 d_2}{32\pi \Lambda_1^2 \rho_2}, \tag{56}$$

where the first term on the right-hand side is the Bardeen-Stephen drag coefficient for a vortex in the S film, and the second term is the inductive drag coefficient η_2 due to the metallic overlayer. Here η_2 is consistent up to a numerical factor ~ 1 with the result of Ref. ([39]) obtained in the limit of $d_i = 0$. As shown in Appendix D, η_2 turns out to be independent of the gap width d_i as long as $d_i + d_2 \ll \min(w, \Lambda)$. Although η_2 appears similar to η_1 with the replacement $\rho_2 \to \rho_1$ and $\xi \to \Lambda$, the inductive heating in the overlayer actually occurs in a small region of radius $\sim d_i + d_1 \ll w$. Here the factor Λ^{-2} in η_2 does not result from magnetic screening but comes from the magnitude of the vortex sheet current in the moving Pearl vortex [45], which induces eddy currents in the overlayer.

Very thin films have $\Lambda^2 \gg \xi^2$, so η_2 is generally much smaller than η_1, even for highly conductive overlayers with $\rho_2 \ll \rho_1$. The ratio of the inductive and viscous drag coefficients is

$$\frac{\eta_2}{\eta_1} \simeq \frac{d_1 d_2 \rho_1}{40 \kappa^4 \xi^2 \rho_2}, \tag{57}$$

where $\kappa = \lambda_L / \xi$ is the GL parameter. For the amorphous MoGe films with $\kappa \sim 100$, $\xi \simeq 25(1 - T/T_c)^{-1/2}$ nm, $\rho_1 \simeq 200$ $\mu\Omega$ cm [87], $d_1 = 3$ nm, and the Au overlayer with $d_2 = 40$ nm and $\rho_2 = 22$ nΩ cm investigated in Ref. [37], Eq. (57) gives $\eta_2 / \eta_1 \sim 10^{-6}$.

VIII. DISCUSSION

The resistive transition temperature in thin superconducting films can be tuned by overlayers that ameliorate pair-breaking fluctuation of vortices and shift T_r back to the mean-field T_c. Revealing the actual T_c of a new 2D superconductor could be done using (i) S-I-S′ trilayers in which a known higher-T_c superconductor S′ is deposited onto a new superconductor S separated by a thin dielectric layer, (ii) a bilayer in which a lower-T_c superconductor or normal overlayer with high carrier density or normal state conductivity is deposited onto a superconducting film, or (iii) metallic or superconducting overlayers that are capacitively or inductively coupled with the main superconducting film. The first two approaches rely on static mechanisms, which increase the energies of vortices. The third approach is based on dynamic mechanisms that affect quantum fluctuations and increase the vortex drag, making vortices less mobile.

(i) S-I-S′ trilayers could be used to reveal T_c of new materials (for instance, FeSe single layers) using high-T_c overlayers. In this case, the current is injected into the S layer and spreads along both layers over the Josephson length L_J, which determines the scale of current redistribution. The solution for the phase difference $\chi(x) = \chi_2 - \chi_1$ obtained in Appendix D is

$$\tan \frac{\chi}{4} = \frac{I e^{-x/L_J}}{I_b + \sqrt{I_b^2 - I^2}}, \tag{58}$$

$$I_g = \frac{2 d_1 g_1}{L_J}, \quad L_J = \left[\frac{d_1 d_2 g_1 g_2}{(d_1 g_1 + d_2 g_2) J_c} \right]^{1/2}. \tag{59}$$

Here J_c is the Josephson current density through the interface, and the phase conductivities g_1 and g_2 define the current

densities $\mathbf{J}_1 = g_1 \nabla \chi_1$ and $\mathbf{J}_2 = g_2 \nabla \chi_2$ in the layers 1 and 2 due to the respective phase gradients $\nabla \chi_1$ and $\nabla \chi_2$. For dirty s-wave superconductors, $g_i = (\pi \Delta_i \sigma_i / 2e) \tanh(\Delta_i / 2T)$, $i = 1, 2$. At $I > I_b$, the current injected into the layer 1 generates interlayer phase slips [88]. Therefore, the S′ layer does not short circuit the S layer if $I < I_b$, and the length of the bridge is shorter than L_J.

A higher-T_c overlayer increases the energy barriers for the BKT proliferation or thermally activated hopping of perpendicular vortices, depending on the overlayer thickness d_2, as illustrated in Fig. 2. At small $d_2 < d_{2c}$, the overlayer increases the phase stiffness and the energies of complete vortices threading both layers, so that $T_r(d_2)$ increases with d_2 up to the critical thickness d_{2c} defined by Eq. (17). At $d_2 > d_{2c}$, partial vortices in layer 1 become more energetically favorable and the overlayer increases the energy of the vortex by the amount of the Josephson energy proportional to the area of the bridge, so that T_r becomes independent of d_2. The maximum value of T_r at $d_2 > d_{2c}$ can be reached by changing the bridge dimensions and the interlayer J_c.

(ii) The resistive transition temperature T_r can be increased in a bilayer with a proximity-coupled overlayer that can be either normal or superconducting. Here partial vortices are not energetically favorable, but the overlayer increases the total sheet superfluid density and thus the energy of complete vortices while decreasing the mean-field T_c due to the proximity effect. As was shown above, the interplay of these trends yields a nonmonotonic dependence of T_r and the BKT transition temperature on the overlayer thickness.

The maximum T_r close to the mean-field T_c could be reached by depositing a thin normal layer with $d_2 \ll d_1$, where the optimum thickness d_{2m} estimated by Eq. (42) turns out to be independent of σ_1 if $\sigma_2 \gg \sigma_1$. This condition is satisfied for good metals such as Ag, Cu, or Au with $\sigma_2 \sim (10^3 - 10^4) \sigma_1$ as compared to typical values of σ_1 for cuprates, pnictides, or amorphous low-T_c monolayers. The proximity-effect reduction of T_c can be ameliorated by the contact resistance between the layers 1 and 2, as shown in Fig. 3. In turn, the contact resistance can be effectively tuned by heat treatment, which can change R_B by several orders of magnitude, as, for example, was shown for the YBCO-Ag interface [89,90].

(iii) Fluctuations in a 2D superconductor can be tuned by its inductive or capacitive coupling with a remote normal or superconducting film. This effect was observed on planar arrays of Al Josephson junctions [36] and MoGe films [37]. Theoretical explanations invoked the ideas of remote gates providing a tunable dissipative environment affecting quantum fluctuations and tunneling of vortices in a superconductor [38,39]. For thermally activated dynamics of vortices considered in this paper, a remote gate causes additional vortex drag due to eddy currents induced in a metallic overlayer [39]. However, the inductive contribution to the vortex drag coefficient η_2 in Eqs. (56) and (57) turns out to be much smaller that the conventional Bardeen-Stephen viscous drag in the superconducting film, particularly in the extreme 2D limit, $\Lambda^2 / \xi^2 \to \infty$. Therefore, despite the proximity effect reduction of T_c, the increase of T_r by direct contact of a superconducting film with a thin, highly conducting normal layer appears far more effective than increasing the vortex drag by inductive coupling.

The approach of this work is based on the conventional Usadel equations assuming that the pairing constants, normal densities of states, and phonon frequencies are independent of the layer thicknesses. This model takes into account neither surface scattering nor interface superconductivity caused by localized phonon modes and changes the pairing constants and DOS at the interface. For instance, a highly conductive overlayer can improve electron screening in the S layer, weakening the Coulomb repulsion and enhancing the Cooper pairing [43,44]. In this case, one would expect that the mean field $T_{c0}(d_2)$ increases as d_2 increases, levels off as d_2 exceeds the Thomas-Fermi screening length l_{TF}, and then decreases at larger d_2 due to the proximity effect. However, the small values of $l_{TF} = 0.5$–0.6 Å for Pb, Cu, Ag, and Au [91] indicate that the effect of screening on T_c becomes independent of the overlayer thickness at $d_2 \gtrsim 1$ Å. In this case, screening may not explain the nonmonotonic dependence of $T_r(d_2)$ with maxima at 2–4 Å $\gg l_{TF}$ observed on Bi-(Au, Ag), Ga-Ag, and Pb-Ag bilayers [30–33]. The maxima in $T_r(d_2)$ at $d_2 \gg l_{TF}$ readily follow from the vortex mechanism suggested in this work.

Overlayers can be used to tune the BKT transition and reveal the effect of different materials parameters, particularly inhomogeneities [54,55], DOS broadening, and surface and interface scattering. Given the significant DOS broadening observed by tunneling experiments on ultrathin films [33,56–59], the pair-breaking DOS broadening effects can contribute to the observed reduction of both T_c and T_b. Since the DOS broadening affects T_c and T_b differently, it cannot be just taken into account by substituting the observed T_c into Eq. (1) to infer T_b from the experiment.

The BKT transition temperature depends on the factor ζ affected by multiple mechanisms contributing to the renormalization of the superfluid density and electron diffusivity by effects of strong electron-phonon coupling [77–79], fluctuations and weak localization [49]. Moreover, ζ can be affected by such uncertain material factors as inhomogeneities of superconducting properties, defects that pin vortices, crystalline granularity, DOS broadening, surface scattering, and finite-size effects. Thus, the actual evaluation of $T_b(d_2)$ controlled by the resistance ratio $r = 8R_0/\pi \zeta R$ can only be done if ζ is regarded as a material parameter that could be expressed via the observed T_b of a bare film at $d_2 = 0$. This paper focuses on the qualitative effects of the overlayer on the resistive transition temperature, which was quantified by either $T_b(d_2)$ or $T_r(d_2)$ for single-vortex hopping. It turned out that both $T_b(d_2)$ and $T_r(d_2)$ exhibit similar dependencies on d_2, so the main conclusion of this work about the mitigation of vortex fluctuations by overlayers is not that sensitive to the resistance criterion for T_r. Other factors, such as the effect of the vortex core on the BKT transition in a bilayer where the core size given by Eq. (39) depends on d_2 and can be much larger than ξ_1 in the S film, deserve a more detailed investigation.

APPENDIX A: CRITICAL TEMPERATURE OF A BILAYER

In the Cooper limit, $\theta_{1,2}(x)$ are nearly uniform across the layers, so that the quadratic expansions can be used:

$$\theta_1(x) = \theta_1 - C_1(x + d_1)^2, \tag{A1}$$

$$\theta_2(x) = \theta_2 + C_2(x - d_2)^2. \tag{A2}$$

The solution of Eqs. (18)–(22) at $C_1 d_1^2 \ll 1$ and $C_2 d_2^2 \ll 1$ is

$$C_1 D_1 = \Delta_1 \cos\theta_1 - \omega_1 \sin\theta_1, \tag{A3}$$

$$C_2 D_2 = \omega_2 \sin\theta_2 - \Delta_2 \cos\theta_2, \tag{A4}$$

$$C_1 d_1 \sigma_1 = C_2 d_2 \sigma_2, \tag{A5}$$

$$C_2 d_2 \sigma_2 = R_B^{-1}(\sin\theta_1 \cos\theta_2 - \cos\theta_1 \sin\theta_2), \tag{A6}$$

where $\omega_{1,2} = \omega + \Gamma_{1,2}$. Solving for C_1 and C_2 yields Eqs. (23)–(25). At negligible contact resistance $R_B \to 0$, Eqs. (A3)–(A6) give $\theta_1 = \theta_2 \equiv \theta$, and

$$\sin\theta = \frac{\Delta}{\sqrt{(\omega + \Gamma)^2 + \Delta^2}}, \tag{A7}$$

$$\Delta = \frac{\Delta_1 + \alpha \Delta_2}{1 + \alpha}, \quad \Gamma = \frac{\Gamma_1 + \alpha \Gamma_2}{1 + \alpha}, \quad \alpha = \frac{d_2 N_2}{d_1 N_1}. \tag{A8}$$

The equations for Δ_1 and Δ_2 become

$$\Delta_1 = 2\pi T \lambda_1 \sum_{\omega>0}^{\Omega_1} \frac{\Delta}{\sqrt{(\omega + \Gamma)^2 + \Delta^2}}, \tag{A9}$$

$$\Delta_2 = 2\pi T \lambda_2 \sum_{\omega>0}^{\Omega_2} \frac{\Delta}{\sqrt{(\omega + \Gamma)^2 + \Delta^2}}. \tag{A10}$$

Multiplying Eq. (A9) by $1/(1 + \alpha)$ and Eq. (A10) by $\alpha/(1 + \alpha)$ and adding them gives a single equation for Δ:

$$1 = \sum_{\omega>0}^{\Omega_1} \frac{2\pi T \tilde{\lambda}_1}{\sqrt{(\omega + \Gamma)^2 + \Delta^2}} + \sum_{\omega>0}^{\Omega_2} \frac{2\pi T \tilde{\lambda}_2}{\sqrt{(\omega + \Gamma)^2 + \Delta^2}}, \tag{A11}$$

where

$$\tilde{\lambda}_1 = \frac{\lambda_1}{1 + \alpha}, \quad \tilde{\lambda}_2 = \frac{\lambda_2 \alpha}{1 + \alpha}. \tag{A12}$$

Taking the limit of $\Delta \to 0$ yields the equation T_c,

$$1 = \sum_{n=0}^{\Omega_1/2\pi T_c} \frac{\tilde{\lambda}_1}{n + \frac{1}{2} + \gamma} + \sum_{n=0}^{\Omega_2/2\pi T_c} \frac{\tilde{\lambda}_2}{n + \frac{1}{2} + \gamma}, \tag{A13}$$

where $\gamma = \Gamma/2\pi T$. The summation in Eq. (A13) is not well defined because the hard cutoffs $\mathcal{N}_{1,2} = \Omega_{1,2}/2\pi T$ are not necessarily integer. Taking only integer parts of $\mathcal{N}_{1,2}$ in numerical calculations can produce spurious contributions in T_c, particularly if $\mathcal{N}_{1,2}$ are not very large for real materials. This issue can be addressed by inserting the bell-shaped functions $S_{1,2}(n) = \mathcal{N}_{1,2}^2/[(n + 1/2)^2 + \mathcal{N}_{1,2}^2]$ and extending the summation over n to infinity. Then Eq. (A13)

becomes

$$1 = \sum_{n=0}^{\infty} \frac{\tilde{\lambda}_1 S_1 + \tilde{\lambda}_2 S_2}{n + \frac{1}{2} + \gamma}. \tag{A14}$$

The summation is done using

$$I = \sum_{n=0}^{\infty} \frac{\mathcal{N}^2}{(n + \frac{1}{2} + \gamma)[(n + \frac{1}{2})^2 + \mathcal{N}^2]}$$
$$= \frac{\mathcal{N}^2}{\mathcal{N}^2 + \gamma^2} \left[\text{Re}\psi\left(\frac{1}{2} + i\mathcal{N}\right) - \psi\left(\frac{1}{2} + \gamma\right) \right.$$
$$\left. + \frac{\pi\gamma}{2\mathcal{N}} \tanh \pi\mathcal{N} \right]. \tag{A15}$$

If $\mathcal{N} \gg \max(\gamma, 1)$, $\text{Re}\psi(\frac{1}{2} + i\mathcal{N}) \simeq \ln \mathcal{N}$ so that

$$I = \ln(4\gamma_E \mathcal{N}) - U(\gamma), \tag{A16}$$

where $U(\gamma)$ is defined by Eq. (9), and $\psi(\frac{1}{2}) = -\ln(4\gamma_E)$. At $\gamma = 0$, Eqs. (A14) and (A16) reproduce the well-known T_{c0} of a bilayer in the Cooper limit [24]:

$$T_{c0} = \frac{2\gamma_E}{\pi} \Omega_1^{1-a} \Omega_2^a e^{-1/\lambda}, \tag{A17}$$

where

$$\lambda = \frac{\lambda_1 + \alpha\lambda_2}{1 + \alpha}, \quad a = \frac{\alpha\lambda_2}{\lambda_1 + \alpha\lambda_2}. \tag{A18}$$

If Γ_1 and Γ_2 are essential, T_c is determined by Eq. (A14), which can be recast in the form

$$1 - \sum_{n=0}^{\infty} \frac{\tilde{\lambda}_1 S_1 + \tilde{\lambda}_2 S_2}{n + \frac{1}{2}} = \lambda \sum_{n=0}^{\infty} \left[\frac{1}{n + \frac{1}{2} + \gamma} - \frac{1}{n + \frac{1}{2}} \right]. \tag{A19}$$

Here the second term on the left-hand side was subtracted from both sides of Eq. (A14). The sum in the right-hand side converges over $n \sim \gamma \ll \mathcal{N}_{1,2}$, so $S_{1,2}(n)$ were set to 1, and $\lambda = \tilde{\lambda}_1 + \tilde{\lambda}_2$ was used. Summing up in Eq. (A19) using Eqs. (A16)–(A18) yields Eq. (8).

If the interface resistance cannot be neglected, Eqs. (23)–(25) for θ_1 and θ_2 can only be solved numerically. A general equation for T_c can be obtained by linearizing Eqs. (23) and (24) with respect to small θ_1 and θ_2:

$$\theta_1 = \frac{\Delta_1(1 + \alpha\beta\omega_2) + \alpha\Delta_2}{(1 + \alpha\beta\omega_2)\omega_1 + \alpha\omega_2}, \tag{A20}$$

$$\theta_2 = \frac{\Delta_1 + \alpha(1 + \beta\omega_1)\Delta_2}{\alpha(1 + \beta\omega_1)\omega_2 + \omega_1}. \tag{A21}$$

Substituting Eqs. (A20) and (A21) into the linearized Eq. (20) and solving the resulting system of linear equations for Δ_1 and Δ_2 yields the following equation for T_c:

$$(1 - \lambda_1 R_{11})(1 - \lambda_2 R_{22}) - \lambda_1\lambda_2 R_{12} R_{21} = 0, \tag{A22}$$

where

$$R_{11} = 2\pi T_c \sum_{\omega>0}^{\infty} \frac{(1 + \alpha\beta\omega_2)S_1(\omega)}{(1 + \alpha\beta\omega_2)\omega_1 + \alpha\omega_2}, \tag{A23}$$

$$R_{22} = 2\pi T_c \sum_{\omega>0}^{\infty} \frac{\alpha(1 + \beta\omega_1)S_2(\omega)}{\alpha(1 + \beta\omega_1)\omega_2 + \omega_1}, \tag{A24}$$

$$R_{12} = 2\pi T_c \sum_{\omega>0}^{\infty} \frac{\alpha S_1(\omega)}{(1 + \alpha\beta\omega_2)\omega_1 + \alpha\omega_2}, \tag{A25}$$

$$R_{21} = 2\pi T_c \sum_{\omega>0}^{\infty} \frac{S_2(\omega)}{\alpha(1 + \beta\omega_1)\omega_2 + \omega_1}. \tag{A26}$$

Equations (A22)–(A26), which contain rapidly converging sums, are rather suitable for numerical calculations of T_c depending on the multitude of materials parameters $\lambda_{1,2}, d_{1,2}, N_{1,2}, \Gamma_{1,2}, R_B$.

For a normal overlayer with $\lambda_2 = 0$, the equation for T_c takes the form (30). If $\Gamma_1 = \Gamma_2 = 0$, this equation can be reduced to

$$\frac{1}{\lambda_1} = \frac{1}{1 + \alpha} \sum_{n=0}^{\infty} \left[\frac{1}{n_1} + \frac{\alpha}{n_1 + \mathcal{M}} \right] \frac{\mathcal{N}^2}{n_1^2 + \mathcal{N}^2}, \tag{A27}$$

where $n_1 = n + 1/2$, $\mathcal{N} = \Omega_1/2\pi T$, and $\mathcal{M} = (1 + \alpha)/2\pi\alpha\beta T$. Summation in Eq. (A27) can be done using Eq. (A15). In the BCS limit $\mathcal{N} \gg 1$, one can use $\text{Re}\psi(1/2 + i\mathcal{N}) \to \ln \mathcal{N}$ so that Eq. (A27) becomes

$$\frac{1 + \alpha}{\lambda_1} = \ln \frac{2\gamma_E \Omega_1}{\pi T} + \frac{\alpha\mathcal{N}^2}{\mathcal{N}^2 + \mathcal{M}^2}$$
$$\times \left[\ln \frac{2\gamma_E \Omega_1}{\pi T} + \frac{\pi\mathcal{M}}{2\mathcal{N}} - U(\mathcal{M}) \right]. \tag{A28}$$

Using here $(1 + \alpha)/\lambda_1 = \ln(2\gamma_E \Omega_1/\pi T_{c0})$, where $T_{c0} = T_{c1} \exp(-\alpha/\lambda_1)$ is the critical temperature of an N-S bilayer with $R_B = 0$, yields Eq. (31).

It is instructive to compare T_c described by Eq. (31) with T_c obtained using the BCS hard cutoff at $\omega = \Omega_1$, in which case Eq. (A27) is truncated to

$$\frac{1}{\lambda_1} = \frac{1}{1 + \alpha} \sum_{n=0}^{\mathcal{N}} \left[\frac{1}{n_1} + \frac{\alpha}{n_1 + \mathcal{M}} \right]. \tag{A29}$$

Hence,

$$\frac{1 + \alpha}{\lambda_1} = \psi\left(\frac{3}{2} + \mathcal{N}\right) - \psi\left(\frac{1}{2}\right)$$
$$+ \alpha\left[\psi\left(\frac{3}{2} + \mathcal{M} + \mathcal{N}\right) - \psi\left(\frac{1}{2} + \mathcal{M}\right)\right]. \tag{A30}$$

In the BCS limit $\mathcal{N} \gg 1$, Eq. (A30) yields the following equation, which has been obtained previously [28,29]:

$$\ln \frac{T_c}{T_{c1}} = \frac{\alpha}{1 + \alpha} \left[\ln \left(1 + \frac{1 + \alpha}{\alpha\beta\Omega_1}\right) - U\left(\frac{1 + \alpha}{2\pi\alpha\beta T_c}\right) \right], \tag{A31}$$

where the logarithmic term in the brackets, which provides the correct limit $T_c \to T_{c0}(\alpha)$ at $R_B \to 0$, is only essential at small α and β for which $\mathcal{M} \gg 1$. Numerical solutions show that both $T_c(\alpha)$ described by Eqs. (31) and (A31) have very similar dependencies on α. For the case shown in Fig. 3, the largest difference ($\lesssim 9\%$) between $T_c(\alpha)$ calculated from Eqs. (31) and (A31) occurs at $2\pi\beta T_{c1} = 3$ and $\alpha \simeq 1$.

APPENDIX B: FREE ENERGY, GL FUNCTIONAL, VORTEX CORE ENERGY, AND VISCOSITY

The free energy of a dirty bilayer is given by

$$F = \int (f_1 + f_2)d^2\mathbf{r}, \tag{B1}$$

$$f_l = \frac{\nu_l \Delta_l^2}{\lambda_l} + 4\pi T n_l \sum_{\omega>0}^{\Omega_l} \left[\omega(1 - \cos\theta_l) - \Delta_l \sin\theta_l \right.$$
$$\left. + \frac{D_l}{2} Q^2 \sin^2\theta_l + \frac{D_l}{2}(\nabla\theta_l)^2 \right], \tag{B2}$$

where $\nu_i = d_i N_i$, $\mathbf{Q} = \nabla\chi + 2\pi\mathbf{A}/\phi_0$, $\chi_l(\mathbf{r})$ is the phase of the order parameter, $\Psi_l(\mathbf{r}) = \Delta_l(\mathbf{r})e^{i\chi_l(\mathbf{r})}$, and $l = 1,2$. For a strongly coupled bilayer with $\alpha\beta\Omega_{1,2} \ll 1$ and no DOS broadening, $\theta_1 = \theta_2 = \theta$ and Eq. (20) yields

$$\lambda_1\Delta_2 = \lambda_2\Delta_1, \quad \nu\Delta = \nu_1\Delta_1 + \nu_2\Delta_2, \tag{B3}$$

$$\Delta_1 = \frac{\lambda_1}{\lambda}\Delta, \quad \Delta_2 = \frac{\lambda_2}{\lambda}\Delta, \tag{B4}$$

$$\Delta = \frac{\nu_1\Delta_1 + \nu_2\Delta_2}{\nu_1 + \nu_2}, \quad \lambda = \frac{\lambda_1\nu_1 + \lambda_2\nu_2}{\nu_1 + \nu_2}, \tag{B5}$$

where $\nu = \nu_1 + \nu_2$. From Eqs. (B3)–(B5), it follows that

$$\frac{\nu_1\Delta_1^2}{\lambda_1} + \frac{\nu_2\Delta_2^2}{\lambda_2} = \frac{\nu\Delta^2}{\lambda}. \tag{B6}$$

Using Eqs. (B3)–(B6) and Eqs. (A17) and (A18) for T_{c0}, the free energy in Eqs. (B1) and (B2) for a phase-locked bilayer can be expressed in terms of a single order parameter Δ, the combined sheet density of states $\nu = d_1 N_1 + d_2 N_2$, and an effective diffusivity D:

$$F = \nu \int \left\{ \Delta^2 \ln\frac{T}{T_{c0}} + 4\pi T \sum_{\omega>0} \left[\omega(1 - \cos\theta) - \Delta\sin\theta \right.\right.$$
$$\left.\left. + \frac{\Delta^2}{2\omega} + \frac{D}{2}Q^2\sin^2\theta + \frac{D}{2}(\nabla\theta)^2 \right] \right\} d^2\mathbf{r}, \tag{B7}$$

$$D = \frac{\nu_1 D_1 + \nu_2 D_2}{\nu_1 + \nu_2}. \tag{B8}$$

Variation of F with respect to $\delta\theta$ and $\delta\Delta$ results in the mean-field Usadel equations,

$$2\omega\sin\theta + D(Q^2\sin\theta\cos\theta - \nabla^2\theta) = 2\Delta\cos\theta, \tag{B9}$$

$$\Delta\ln\frac{T}{T_{c0}} = 2\pi T \sum_{\omega>0} \left(\sin\theta - \frac{\Delta}{\omega} \right). \tag{B10}$$

The GL equations are obtained by expanding Eq. (B9) in small gradients and powers of Δ at $T \approx T_c$:

$$\theta \approx \frac{\Delta}{\omega} + \frac{D}{2\omega^2}(\nabla^2\Delta - Q^2\Delta) - \frac{\Delta^3}{3\omega^3}. \tag{B11}$$

Substituting this into Eq. (B7) and summing up over ω yields the GL functional (33)–(35).

A fluctuation contribution to the specific heat $\delta C(T)$ at $T > T_{c0}$ is obtained by expanding Eq. (B7) to quadratic terms in the Fourier components Ψ_k:

$$\delta F = A\nu \int \frac{d^2\mathbf{k}}{(2\pi)^2} \left[\left(\ln\frac{T}{T_{c0}} + \frac{\hbar Dk^2}{8T_{c0}} \right)|\Psi_k|^2 \right], \tag{B12}$$

where A is the bilayer area. The Gaussian fluctuation correction [76] to the statistical sum $\delta Z = \int e^{-\delta F/T} D\Psi_k$ yields Eq. (36) for $\delta C = -T\partial^2 \ln Z/\partial T^2$.

The condensation energy density f_0 of a uniform state is obtained by expressing $\Delta \ln(T/T_{c0})$ in Eq. (B7) in terms of the ω-sum from Eq. (B10):

$$f_0 = 2\pi T \sum_{\omega>0} \frac{\nu\Delta^4}{\sqrt{\omega^2 + \Delta^2}(\omega + \sqrt{\omega^2 + \Delta^2})^2}. \tag{B13}$$

Here $f_0 = H_c^2/8\pi$ defines the thermodynamic critical field H_c of a bilayer. At $T \approx T_{c0}$, the gap Δ in the denominator of Eq. (B13) can be dropped giving

$$f_0 = \frac{7\zeta(3)\nu\Delta^4}{16\pi^2 T_{c0}^2}. \tag{B14}$$

The energy of the vortex core ϵ_c may be evaluated by writing the total energy of a vortex in the form

$$\epsilon = \epsilon_0 \ln\frac{L}{\xi} + 2\pi\xi^2 f_0, \tag{B15}$$

where $\epsilon_0 = (\pi^2/2)\hbar\nu D\Delta \tanh(\Delta/2T)$ follows from Eq. (45) at $\Gamma = 0$, and the term $2\pi\xi^2 f_0$ accounts for the loss of condensation energy in a normal core of radius $\simeq \sqrt{2}\xi$ [92]. The composite coherence length ξ can be obtained by minimizing $\epsilon(\xi)$ with respect to ξ:

$$\epsilon = \epsilon_0 \left(\ln\frac{L}{\xi} + \frac{1}{2} \right), \quad \epsilon_c = \frac{\epsilon_0}{2}, \tag{B16}$$

$$\xi = (\epsilon_0/4\pi f_0)^{1/2}. \tag{B17}$$

Using here $\epsilon_0 = \pi^2\hbar D\nu\Delta^2/4T_{c0}$, $\Delta^2(T) = 8\pi^2 T_{c0}(T_{c0} - T)/7\zeta(3)$, and f_0 from Eq. (B14) at $T \approx T_{c0}$ yields

$$\xi = \left[\frac{\pi\hbar D}{8(T_{c0} - T)} \right]^{1/2}. \tag{B18}$$

For a single film, Eq. (B16) is consistent with $\epsilon_c \approx 0.497\epsilon_0$ obtained from numerical simulation of a single vortex [52], and Eq. (B18) reproduces the GL coherence length $\xi = \sqrt{c/|a|}$, with a and c given by Eqs. (33)–(35). This qualitative analysis shows that both $\epsilon_c \propto (d_1\sigma_1 + d_2\sigma_2)$ and the core radius $\xi \propto (d_1\sigma_1 + d_2\sigma_2)^{1/2}$ of a vortex in a bilayer can be significantly increased by a conductive overlayer with $\sigma_2 \gg \sigma_1 d_1/\sigma_2$.

The viscous drag coefficient η of a vortex in a bilayer can be evaluated from the power balance $\eta v^2 B/\phi_0 = E^2/R_F$. Here the velocity v of vortices with the areal density B/ϕ_0 is related to the electric field E in the core by the Faraday law $E = vB$, $R_F = R_\square B/B_{c2}$ is the flux flow sheet resistance, $R_\square = (d_1\sigma_1 + d_2\sigma_2)^{-1}$, and $B_{c2} = \phi_0/2\pi\xi^2$. Hence η acquires the conventional Bardeen-Stephen form $\eta = \phi_0^2/2\pi\xi^2 R_\square$. Expressing here $R_\square$ and ξ in terms of the bilayer parameters yields

$$\eta = 8\hbar(d_1 N_1 + d_2 N_2)(T_{c0} - T). \tag{B19}$$

Here η is independent of the mean free path in both N and S layers, consistent with the behavior of the Bardeen-Stephen

drag coefficient $\eta_{BS} = 8\hbar N(T_{c0} - T)$ per unit vortex length in the dirty limit at $T \approx T_c$ [51].

APPENDIX C: CURRENT DISTRIBUTION IN A PARTIAL VORTEX

A vortex in a thin-film strip in which the London screening is negligible ($d \ll \lambda_L$) can be described by the complex potential [81,82],

$$g(z) = \chi(x,y) + ih(x,y) = i \ln \frac{\sin \frac{\pi}{2w}(z+u)}{\sin \frac{\pi}{2w}(z-u)}, \quad \text{(C1)}$$

$$J_x - iJ_y = -\frac{\phi_0}{2\mu_0 \Lambda} \frac{dg}{dz}, \quad \text{(C2)}$$

where $z = x + iy$, the strip is at $0 < x < w$ and infinite along y, $\Lambda = \lambda_L^2/d$, and the vortex core is at $x = u$, $y = 0$. Both components of the sheet current density $J_x(x,y)$ and $J_y(x,y)$ circulating around the vortex decrease exponentially over the length w/π along the strip [81],

$$J_x(x,y) = \frac{\phi_0}{4\mu_0 \Lambda w} \left[\frac{\sinh \frac{\pi y}{w}}{\cosh \frac{\pi y}{w} - \cos \frac{\pi}{w}(x+u)} \right.$$
$$\left. - \frac{\sinh \frac{\pi y}{w}}{\cosh \frac{\pi y}{w} - \cos \frac{\pi}{w}(x-u)} \right], \quad \text{(C3)}$$

$$J_y(x,y) = \frac{\phi_0}{4\mu_0 \Lambda w} \left[\frac{\sin \frac{\pi}{w}(x-u)}{\cosh \frac{\pi y}{w} - \cos \frac{\pi}{w}(x-u)} \right.$$
$$\left. - \frac{\sin \frac{\pi}{w}(x+u)}{\cosh \frac{\pi y}{w} - \cos \frac{\pi}{w}(x+u)} \right]. \quad \text{(C4)}$$

The function $\chi(x,y)$ in Eq. (C1) is the phase of the order parameter, which is in turn the phase difference between the superconducting film and the overlayer with no current. The phase χ results in the Josephson energy:

$$W_J = \frac{\hbar J_c}{2e} \int_0^w dx \int_{-L/2}^{L/2} dy [1 - \cos \chi(x,y)]. \quad \text{(C5)}$$

Separation of the real part in Eq. (C1) yields

$$\chi = \tan^{-1} \frac{\tanh \frac{\pi y}{2w}}{\tan \frac{\pi}{2w}(x-u)} - \tan^{-1} \frac{\tanh \frac{\pi y}{2w}}{\tan \frac{\pi}{2w}(x+u)}. \quad \text{(C6)}$$

As follows from Eq. (C6), the vortex causes a nonzero phase $\chi_\infty(x)$ at $|y| \gg w/\pi$. If $y \to \infty$, Eq. (C6) yields $\chi_\infty(x) = \pi u/w$ at $u < x < w$, $\chi_\infty(x) = \pi(u/w - 1)$ at $0 < x < u$, and $\chi(x,\infty) = -\chi(x,-\infty)$. This form of $\chi_\infty(x)$ yields a discontinuity in the Josephson current density $\pm J_c \sin(\pi u/w)$ at $x = u$ across the bilayer. The discontinuity in $J_c \sin \chi$ can be removed by choosing a branch cut at $x = 0$ and $-\infty < y < 0$, giving

$$\chi_\infty(x) = 2\pi u/w, \quad y \to \infty, \quad \text{(C7)}$$

$$\chi_\infty(x) = 2\pi, \quad 0 < x < u, \quad y \to -\infty, \quad \text{(C8)}$$

$$\chi_\infty(x) = 0, \quad u < x < w, \quad y \to -\infty. \quad \text{(C9)}$$

The function $\chi(x,y)$ is shown in Fig. 9. The constant phase difference χ_∞ at $y \gg w/\pi$ produces the Josephson energy
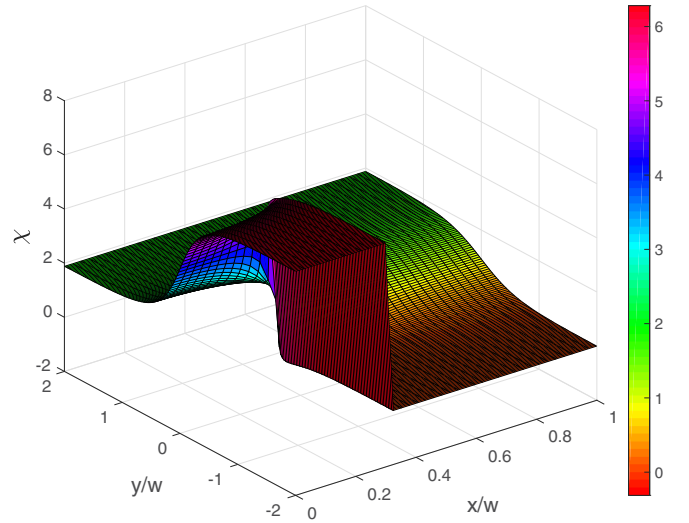

FIG. 9. The surface plot of $\chi(x,y)$ calculated from Eq. (C6) with the branch cut at $x = 0$ and $-\infty < y < 0$ for a vortex at $u = 0.3w$.

proportional to the film area:

$$W_J = \frac{\hbar J_c}{4e} L w \left(1 - \cos \frac{2\pi u}{w}\right). \quad \text{(C10)}$$

The finite phase difference χ_∞ at $y \gg w$ causes a transverse Josephson current $\sim J_c w$ that spreads through the layers 1 and 2. A self-consistent calculation of the phase distributions $\chi_1(\mathbf{r})$ and $\chi_2(\mathbf{r})$ in both layers requires solving the sine-Gordon equation obtained in Appendix E along with Eq. (C1).

APPENDIX D: VORTEX INDUCTIVE DRAG CAUSED BY A METALLIC OVERLAYER

A moving Pearl vortex produces the azimuthal vector potential $A_\varphi(x,y)$ outside a thin film [45]:

$$A_\varphi(R) = \frac{\phi_0}{2\pi} \int_0^\infty \frac{J_1(kR)e^{-k|z|}}{1 + 2k\Lambda} dk, \quad \text{(D1)}$$

where $\Lambda = \lambda_L^2/d_1$, $R = \sqrt{(x-u)^2 + y^2}$, $u(t)$ is a time-dependent coordinate of the vortex core, and $J_1(x)$ is the Bessel function. The main contribution to the inductive drag comes from the region of radius $R \sim (d_2 + d_i) \ll \min(w,\Lambda)$ around the vortex, so the integral (D1) is dominated by $k\Lambda \gg 1$. In this case,

$$A_\varphi(R) = \frac{\phi_0}{4\pi \Lambda} \int_0^\infty \frac{J_1(kR)}{k} e^{-k|z|} dk$$
$$= \frac{\phi_0 R}{4\pi \Lambda(|z| + \sqrt{R^2 + z^2})}. \quad \text{(D2)}$$

The inductive electric field $E_\varphi(R) = -\dot{A}_\varphi$ produced by the moving vortex outside the film is then

$$E_\varphi(x,y,z,t) = \frac{\dot{u}\phi_0(x-u)|z|}{4\pi \Lambda R \sqrt{R^2 + z^2}(|z| + \sqrt{R^2 + z^2})}. \quad \text{(D3)}$$

Let the vortex move with a slowly varying velocity $\dot{u}(t)$ that only has low-frequency Fourier harmonics for which the skin depth, $(\mu_0 \sigma_2 \omega)^{-1/2}$, is much larger than d_2. Then

screening of a transverse electromagnetic field is negligible, so the inductive electric field $E_\varphi(R,z,t)$ of the vortex penetrates freely into the N overlayer. In this case, Eq. (D3) can be used to calculate the Ohmic power $P = \sigma_2 \int_{V_2} E^2 dx\, dy\, dz$ in the N overlayer spaced by d_i from the S film. Consider first the power density $p(z) = \sigma_2 \int E^2 dx\, dy$ at the distance z from the film and calculate the integral in polar coordinates centered in the moving vortex core:

$$p(z) = \frac{\dot{u}^2 \phi_0^2 \sigma_2 z^2}{16\pi^2 \Lambda^2} \int_0^{2\pi} \int_0^\infty \frac{R \cos^2 \varphi d\varphi dR}{(R^2 + z^2)(|z| + \sqrt{R^2 + z^2})^2}.$$
(D4)

The main contribution to this integral comes from $R \sim z \sim d_i + d_2$, so the lateral size of the overlayer does not affect $p(z)$ if $d_i + d_2 \ll w$. Integration in Eq. (D4) gives

$$p(z) = \frac{\dot{u}^2 \phi_0^2 \sigma_2}{32\pi \Lambda^2}(\ln 4 - 1).$$
(D5)

Since $p(z)$ turns out to be independent of z, the total power $P = \int_{d_i}^{d_i + d_2} p(z)dz$ is proportional to d_2:

$$P = \frac{\dot{u}^2 \phi_0^2 \sigma_2 d_2}{32\pi \Lambda^2}(\ln 4 - 1).$$
(D6)

Here P is independent of the gap width d_i as long as $d_i + d_2 \ll \min(w, \Lambda)$. In turn, the power P can also be expressed in terms of the inductive vortex drag coefficient η_2 according to $\eta_2 \dot{u}^2 = P$. Hence,

$$\eta_2 = \frac{\phi_0^2 \sigma_2 d_2 d_i^2}{32\pi \lambda_L^4}(\ln 4 - 1).$$
(D7)

APPENDIX E: CURRENT FLOW IN A PHASE-UNLOCKED BILAYER

Consider a bilayer that carries the net current I:

$$I = d_1 J_1 + d_2 J_2.$$
(E1)

Here the current densities in the layers 1 and 2 are related to the respective phase gradients as follows:

$$\mathbf{J}_1 = g_1 \nabla \chi_1, \quad \mathbf{J}_2 = g_2 \nabla \chi_2.$$
(E2)

If $J_1(x)$ varies slowly along the layer 1 over the length $\sim d_1$, the condition of current continuity becomes

$$d_1 \nabla \cdot \mathbf{J}_1 + J_\perp = 0,$$
(E3)

where $J_\perp = J_c \sin \chi + R_i^{-1} V + C_i \partial_t V$ is the current density flowing through the interface. Hence,

$$d_1 g_1 \nabla^2 \chi_1 = J_c \sin \chi + R_i^{-1} V + C_i \partial_t V,$$
(E4)

where $V = (\hbar/2e)\partial_t \chi$ is the Josephson voltage, and $\chi = \chi_2 - \chi_1$ is the phase difference between the layers. From Eqs. (E1) and (E2), it follows that $(d_1 g_1 + d_2 g_2)\nabla^2 \chi_1 = d_2 g_2 \nabla^2 \chi$. Substituting this into Eq. (E4) yields the sine-Gordon equation for $\chi(\mathbf{r}, t)$:

$$\omega_J^{-2} \partial_{tt} \chi + \tau \partial_t \chi = L_J^2 \nabla^2 \chi - \sin \chi,$$
(E5)

where $L_J^2 = d_1 d_2 g_1 g_2/(d_1 g_1 + d_2 g_2)J_c$, $\omega_J^2 = 4e^2 J_c/\hbar^2 C_i$, $\tau = \hbar/2eR_i$, and R_i and C_i are the resistance and capacitance per unit area of the interface, respectively.

A stationary solution of Eq. (E5) that describes the current I injected in the layer 1 at $x = 0$ is

$$\tan \frac{\chi}{4} = Ae^{-x/L_J},$$
(E6)

where A is obtained from the boundary condition, $J_2(0) = 0$, $I = -d_1 g_1 \chi'(0)$. Then Eq. (E6) yields

$$\frac{I}{4g_1 d_1}(1 + A^2) = \frac{A}{L_J}.$$
(E7)

The solution of Eq. (E7) for which $A = 0$ at $I = 0$ is

$$A = \frac{2g_1 d_1}{I L_J} - \sqrt{\left(\frac{2d_1 g_1}{I L_J}\right)^2 - 1}$$
(E8)

Equations (E6) and (E8) yield Eq. (58).

[1] S. Z. Butler, S. M. Hollen, L. Cao, Y. Cui, J. A. Gupta, H. R. Gutiérrez, T. F. Heinz, S. S. Hong, J. Huang, A. F. Ismach, E. Johnston-Halperin, M. Kuno, V. V. Plashnitsa, R. D. Robinson, R. S. Ruoff, S. Salahuddin, J. Shan, L. Shi, M. G. Spencer, M. Terrones, W. Windl, and J. E. Goldberger, ASC Nano **7**, 2898 (2013).

[2] I. Bozovic and C. Ahn, Nat. Phys. **10**, 892 (2014).

[3] Y. Saito, T. Nojima, and Y. Iwasa, Supercond. Sci. Technol. **29**, 093001 (2016).

[4] D. Huang and J. E. Hoffman, Annu. Rev. Condens. Mater. Phys. **8**, 311 (2017).

[5] T. Uchihashi, Supercond. Sci. Technol. **30**, 013003 (2017).

[6] D.-H. Lee, Annu. Rev. Condens. Mater. Phys. **9**, 261 (2018).

[7] Q. Y. Wang, L. Zhi, Z. Wen-Hao, Z. Zuo-Cheng, Z. Jin-Song, L. Wei, D. Hao, O. Yun-Bo, D. Peng, and C. Kai, Chin. Phys. Lett. **29**, 037402 (2012).

[8] S. He, J. He, W. Zhang, L. Zhao, D. Liu, X. Liu, D. Mou, Y. B. Ou, Q. Y. Wang, Z. Li, L. Wang, Y. Peng, Y. Liu, C. Chen, L. Yu, G. Liu, X. Dong, J. Zhang, C. Chen, Z. Xu, X. Chen, X. Ma, Q. Xue, and X. J. Zhou, Nat. Mater. **12**, 605 (2013).

[9] Y. Sun, W. Zhang, Y. Xing, F. Li, Y. Zhao, Z. Xia, L. Wang, X. Ma, Q. K. Xue, and J. Wang, Sci. Rep. **4**, 06040 (2014).

[10] J.-F. Ge, Z.-L. Liu, C. Liu, C.-L. Gao, D. Qian, Q.-K. Xue, Y. Liu, and J.-F. Jia, Nat. Mater. **14**, 285 (2015).

[11] S. Tan, Y. Zhang, M. Xia, Z. Ye, F. Chen, X. Xie, R. Peng, D. Xu, Q. Fan, H. Xu, J. Jiang, T. Zhang, X. Lai, T. Xiang, J. Hu, B. Xie, and D. Feng, Nat. Mater. **12**, 634 (2013).

[12] R. Peng, H. C. Xu, S. Y. Tan, H. Y. Cao, M. Xia, X. P. Shen, Z. C. Huang, C. H. P. Wen, Q. Song, T. Zhang, B. P. Xie, X. G. Gong, and D. L. Feng, Nat. Commun. **5**, 5044 (2014).

[13] J. J. Lee, F. T. Schmitt, R. G. Moore, S. Johnston, Y.-T. Cui, W. Li, M. Yi, Z. K. Liu, M. Hashimoto, Y. Zhang, D. H. Lu, T. P. Devereaux, D.-H. Lee, and Z.-X. Shen, Nature (London) **515**, 245 (2014).

[14] C. Brun, T. Cren, V. Cherkez, F. Debontridder, S. Pons, D. Fokin, M. C. Tringides, S. Bozhko, L. B. Ioffe, B. L. Altshuler, and D. Roditchev, Nat. Phys. **10**, 444 (2014).

[15] S. Yoshizawa, H. Kim, T. Kawakami, Y. Nagai, T. Nakayama, X. Hu, Y. Hasegawa, and T. Uchihashi, Phys. Rev. Lett. **113**, 247004 (2014).

[16] D. Roditchev, C. Brun, L. Serrier-Garcia, J. C. Cuevas, V. H. L. Bessa, M. V. Milošević, F. Debontridder, V. Stolyarov, and T. Cren, Nat. Phys. **11**, 332 (2015).

[17] E. Navarro-Moratalla, J. O. Island, S. Mañas-Valero, E. Pinilla-Cienfuegos, A. Castellanos-Gomez, J. Quereda, G. Rubio-Bollinger, L. Chirolli, J. A. Silva-Guillén, N. Agraït, G. A. Steele, F. Guinea, H. S. J. van der Zant, and E. Coronado, Nat. Commun. **7**, 11043 (2015).

[18] P. Minnhagen, Rev. Mod. Phys. **59**, 1001 (1987).

[19] J. M. Kosterlitz, Rep. Prog. Phys. **79**, 026001 (2016).

[20] E. W. Carson, V. J. Emery, S. A. Kivelson, and D. Orgad, in *Physics of Conventional and Unconventional Superconductivity*, edited by K. H. Bennemann and J. D. Ketterson (Springer-Verlag, Berlin, 2004), Vol. 2, pp. 275–452.

[21] A. Gurevich, Annu. Rev. Condens. Mater. Phys. **5**, 35 (2014).

[22] E. Berg, D. Orgad, and S. A. Kivelson, Phys. Rev. B **78**, 094509 (2008).

[23] G. Wachtel, A. Bar-Yaacov, and D. Orgad, Phys. Rev. B **86**, 134531 (2012).

[24] L. N. Cooper, Phys. Rev. Lett. **6**, 689 (1961).

[25] G. Deutscher and P. G. de Gennes, in *Superconductivity*, edited by R. D. Parks (Marcel Dekker New York, 1969), Vol. 2, pp. 1005–1034.

[26] A. A. Golubov, M. Yu. Kupriyanov, and E. Il'ichev, Rev. Mod. Phys. **76**, 411 (2004).

[27] W. Belzig, C. Bruder, and G. Schön, Phys. Rev. B **53**, 5727 (1996).

[28] Ya. V. Fominov and M. V. Feigelman, Phys. Rev. B **63**, 094518 (2001).

[29] G. Brammertza, A. A. Golubov, P. Verhoeve, R. den Hartog, A. Peacock, and H. Rogalla, Appl. Phys. Lett. **80**, 2955 (2002).

[30] I. L. Landau, D. L. Shapovalov, and I. A. Parshin, Pis'ma Zh. Exp. Teor. Fiz. **53**, 250 (1991) [JETP Lett. **53**, 263 (1991)].

[31] D. L. Shapovalov, Pis'ma Zh. Exp. Teor. Fiz. **60**, 193 (1994) [JETP Lett. **60**, 199 (1994)].

[32] I. L. Landau and I. A. Parshin, Physica B **194–196**, 2339 (1994).

[33] O. Bourgeois, A. Frydman, and R. C. Dynes, Phys. Rev. Lett. **88**, 186403 (2002); Phys. Rev. B **68**, 092509 (2003).

[34] T. Shiino, S. Shiba, N. Sakai, T. Yamakura, L. Jiang, Y. Uzawa, H. Maezawa, and S. Yamamoto, Supercond. Sci. Technol. **23**, 045004 (2010).

[35] O. Yuli, I. Asulin, O. Millo, D. Orgad, L. Iomin, and G. Koren, Phys. Rev. Lett. **101**, 057005 (2008).

[36] A. J. Rimberg, T. R. Ho, C. Kurdak, J. Clarke, K. L. Campman, and A. C. Gossard, Phys. Rev. Lett. **78**, 2632 (1997).

[37] N. Mason and A. Kapitulnik, Phys. Rev. B **65**, 220505(R) (2002).

[38] K.-H. Wagenblast, A. van Otterlo, G. Schön, and G. T. Zimányi, Phys. Rev. Lett. **79**, 2730 (1997).

[39] K. Michaeli and A. M. Finkel'stein, Phys. Rev. Lett. **97**, 117004 (2006); Phys. Rev. B **76**, 064506 (2007).

[40] V. G. Kogan, Phys. Rev. B **75**, 064514 (2007).

[41] A. Gozar and I. Bozovic, Physica C **521–522**, 38 (2016).

[42] X. Y. Tee, T. Ito, T. Ushiyama, Y. Tomioka, I. Martin, and C. Panagopoulos, Phys. Rev. B **95**, 054516 (2017).

[43] A. M. Finkelstein, Physica B **197**, 636 (1994).

[44] Y. Oreg, P. W. Brouwer, B. D. Simons, and A. Altland, Phys. Rev. Lett. **82**, 1269 (1999).

[45] J. Pearl, Appl. Phys. Lett. **5**, 65 (1964); A. L. Fetter and P. C. Hohenberg, Phys. Rev. **159**, 330 (1967).

[46] J. Tobochnik and G. V. Chester, Phys. Rev. B **20**, 3761 (1979).

[47] H. Weber and P. Minnhagen, Phys. Rev. B **37**, 5986 (1988).

[48] A. T. Fiory, A. F. Hebard, and W. I. Glaberson, Phys. Rev. B **28**, 5075 (1983).

[49] E. J. König, A. Levchenko, I. V. Protopopov, I. V. Gornyi, I. S. Burmistrov, and A. D. Mirlin, Phys. Rev. B **92**, 214503 (2015).

[50] A. Erez and Y. Meir, Phys. Rev. B **88**, 184510 (2013).

[51] N. B. Kopnin, *Theory of Nonequilibrium Superconductivity* (Oxford University Press, New York, 2001).

[52] C.-R. Hu, Phys. Rev. B **6**, 1756 (1972).

[53] M. R. Beasley, J. E. Mooij, and T. P. Orlando, Phys. Rev. Lett. **42**, 1165 (1979).

[54] J. Um, B. J. Kim, P. Minnhagen, M. Y. Choi, and S.-I. Lee, Phys. Rev. B **74**, 094516 (2006).

[55] L. Benfatto, C. Castellani, and T. Giamarchi, Phys. Rev. B **80**, 214506 (2009).

[56] J. Zasadzinski, Tunneling spectroscopy of conventional and unconventional superconductors, in *The Physics of Superconductors*, edited by K. H. Bennemann and J. B. Ketterson (Springer, Berlin, 2003), Vol. 1, p. 591.

[57] Z. Long, M. D. Stewart, T. Kouh, and J. M. Valles, Phys. Rev. Lett. **93**, 257001 (2004).

[58] Z. Long, M. D. Stewart, and J. M. Valles, Phys. Rev. B **73**, 140507(R) (2006).

[59] L. Serrier-Garcia, J. C. Cuevas, T. Cren, C. Brun, V. Cherkez, F. Debontridder, D. Fokin, F. S. Bergeret, and D. Roditchev, Phys. Rev. Lett. **110**, 157003 (2013).

[60] R. C. Dynes, V. Narayanamurti, and J. P. Garno, Phys. Rev. Lett. **41**, 1509 (1978).

[61] R. C. Dynes, J. P. Garno, G. B. Hertel, and T. P. Orlando, Phys. Rev. Lett. **53**, 2437 (1984).

[62] T. P. Devereaux and D. Belitz, Phys. Rev. B **44**, 4587 (1991).

[63] D. A. Browne, K. Levin, and K. A. Muttalib, Phys. Rev. Lett. **58**, 156 (1987).

[64] A. N. Bennett, Phys. Rev. **140**, A1902 (1965).

[65] A. I. Larkin and Yu. N. Ovchinnikov, Zh. Exp. Teor. Fiz. **61**, 2147 (1971) [Sov. Phys. JETP **34**, 1144 (1972)].

[66] A. V. Balatskii, I. Vekhter, and J.-X. Zhu, Rev. Mod. Phys. **78**, 373 (2006).

[67] J. S. Meyer and B. D. Simons, Phys. Rev. B **64**, 134516 (2001).

[68] E. L. Wolf and G. B. Arnold, Phys. Rep. **91**, 31 (1982).

[69] M. A. Skvortsov and M. V. Feigel'man, Zh. Eksp. Teor. Fiz. **144**, 560 (2013) [JETP **117**, 487 (2013)].

[70] A. Gurevich and T. Kubo, Phys. Rev. B **96**, 184515 (2017).

[71] R. S. Newrock, C. J. Lobb, U. Geigenmüller, and M. Octavio, Solid State Phys. **54**, 263 (2000).

[72] R. Fazio and H. van der Zant, Phys. Rep. **355**, 235 (2001).

[73] K. K. Likharev, *Dynamics of Josephson Junctions and Circuits* (Gordon and Breach, New York, 1986).

[74] S. John and T. C. Lubensky, Phys. Rev. B **34**, 4815 (1986).

[75] I. S. Beloborodov, A. V. Lopatin, V. M. Vinokur, and K. B. Efetov, Rev. Mod. Phys. **79**, 469 (2007).

[76] A. Larkin and A. Varlamov, *Theory of Fluctuations in Superconductors* (Oxford University Press, New York, 2009).

[77] S. D. Adrian, M. E. Reeves, S. A. Wolf, and V. Z. Kresin, Phys. Rev. B **51**, 6800 (1995).

[78] X. Leyronas and R. Combescot, Phys. Rev. B **54**, 3482 (1996).

[79] E. J. Nicol and J. P. Carbotte, Phys. Rev. B **71**, 054501 (2005).

[80] The renormalized vortex energy should, in principle, be proportional to $\zeta_1 d_1 \sigma_2 + \zeta_2 d_2 \sigma_2$ with two different constants ζ_1 and ζ_2. However, we use here the simpler form given by Eq. (47), assuming that the effects of weak localization in the highly conductive layer 2 would be much less pronounced than in the dirtier layer 1. There are other uncertainties due to, for example, surface and interface scattering, which can be essential in ultrathin films.

[81] G. Stejic, A. Gurevich, E. Kadyrov, D. Christen, R. Joynt, and D. C. Larbalestier, Phys. Rev. B **49**, 1274 (1994).

[82] A. Sheikhzada and A. Gurevich, Phys. Rev. B **95**, 214507 (2017).

[83] A. Gurevich and V. M. Vinokur, Phys. Rev. Lett. **100**, 227007 (2008).

[84] L. Embon, Y. Anahory, A. Suhov, D. Halbertal, J. Cuppens, A. Yakovenko, A. Uri, Y. Myasoedov, M. L. Rappaport, M. E. Huber, A. Gurevich, and E. Zeldov, Sci. Rep. **5**, 7598 (2015).

[85] L. F. Chibotaru and V. H. Dao, Phys. Rev. B **81**, 020502(R) (2010).

[86] Y. Tanaka, H. Yamamori, T. Yanagisawa, T. Nishio, and S. Arisawa, Physica C **548**, 44 (2018).

[87] J. M. Graybeal and M. R. Beasley, Phys. Rev. B **29**, 4167 (1984).

[88] A. Gurevich and V. M. Vinokur, Phys. Rev. Lett. **97**, 137003 (2006).

[89] R. P. Robertazzi, A. W. Kleinsasser, R. B. Laibowitz, R. H. Koch, and K. G. Stawiasz, Phys. Rev. B **46**, 8456 (1992).

[90] J. W. Ekin, S. E. Russek, C. C. Clickner, and B. Jeanneret, Appl. Phys. Lett. **62**, 369 (1993).

[91] N. W. Ashcroft and N. D. Mermin, *Solid State Physics* (Brooks/Cole, Belmont, 1976).

[92] J. R. Clem, J. Low Temp. Phys. **18**, 427 (1975).